KU LEUVEN

FACULTY OF SCIENCE

Mass Transfer Stability of Massive Binaries

The Role of Stellar Structure in Forming Merging Double Compact Objects

Sasha GRAULUS

Supervisor: Prof. P. Marchant
Department of Physics and Astronomy, UGent

Mentor: A. Picco
Institute of Astronomy, KU Leuven

Thesis presented in
fulfillment of the requirements
for the degree of Master of Science
in Astronomy and Astrophysics

Academic year 2024-2025

Preface

Before you lies my master thesis written on the *Mass Transfer Stability of Massive Binaries: The Role of Stellar Structure in Forming Merging Double Compact Objects*. After spending eight wonderful months on this research, I can confidently say that this work has inspired me greatly. Because of this, I would like to thank several people who supported me throughout this journey.

First and foremost, I want to thank my supervisor, Prof. Dr. Pablo Marchant and my mentor, Annachiara Picco, who were my guides throughout this entire research. Thank you both for all your insights, motivation, inspiration, patience, guidance, time, help and everything else. You have mentored me both academically and professionally, and for that, I will forever be grateful. Next, I want to express my gratitude to the entirety of the *Binary Stars* research group for welcoming me every week during the group meetings (and letting me enjoy the free food). A special thank you to the IvS staff and everyone else who was part of my education in Astronomy and Astrophysics.

On a more personal note, I want to thank my partner's parents for letting me be a part of their family for the past five years. Thank you to all my dear friends (especially you, Anne), my mother, brother and sisters. And lastly, there are not enough words to express my gratitude towards my wonderful partner and very soon-to-be fiancé, Dries Ceuppens. It's us in every universe. Thank you for all the support, my love.

To the reader, I hope you enjoy.

Contribution Statement

This thesis is directly built on the work done by my supervisor, Prof. Dr. Pablo Marchant, and my mentor, Annachiara Picco. I performed simulations with version `24.08.1` of the stellar evolution code *Modules for Experiments in Stellar Astrophysics* or `MESA` (Paxton et al., 2011; Paxton et al., 2013; Paxton et al., 2015; Paxton et al., 2018; Paxton et al., 2019; Jermyn et al., 2023). I use the `MESA` single star and binary star physics as described by Marchant et al. (2021). In Chapter 2, we introduce the accretion models. The code to perform the single star evolutions, the code to produce the detailed grid using bisection search and the post-processing code were entirely written by Annachiara Picco with minor adaptations made by me. The accretion experiment described in Chapter 2 was designed by Prof. Dr. Pablo Marchant, Annachiara Picco and me and was performed by me. In Chapter 3, I made adaptations to the binary stellar physics in the `MESA` set-up. All codes to perform and post-process the grid of end-to-end simulations were written and carried out by me. This grid was partially modelled on *Tier-2* of the *Vlaamse Supercomputer Centrum (VSC)*. All input files for the simulations presented in this thesis will be made publicly available on Zenodo[1].

The beautiful image found on the cover page was illustrated by Sara Pinilla. The figure representing a binary evolution (Fig. 1.6) was designed by me, but was inspired by Fig. 1 from Schneider et al. (2023).

This thesis was fully written by me without any help from Generative AI and was proofread by Prof. Dr. Pablo Marchant and Annachiara Picco.

[1] `https://doi.org/10.5281/zenodo.15630075`

Summary

One possible fate of massive binary systems is to evolve into merging double compact objects (CO; i.e., black holes, neutron stars or white dwarfs). These systems are important to study as they are the source of every Gravitational Wave (GW) signal detected by the LIGO-Virgo-Kagra network after their third observational run. The number of detections will substantially grow in the next decennium due to the continuous improvement of current GW detectors and due to future missions (i.e., Laser Interferometer Space Antenna, The Einstein Telescope). However, large uncertainties still exist in our theoretical framework regarding their formation channels, making it challenging to obtain rigorous implications from the current observed sample. It is therefore of extreme importance to have accurate models to complement these detections. In order to produce COs in a tight orbit, binary evolution offers the possibility of reducing the orbital separation significantly through mass transfer from a massive star onto an already formed CO. Recently, it has been shown that *non-conservative stable mass transfer* is able to reduce the orbit of the binary while simultaneously letting the system successfully evolve to a double compact object binary (van den Heuvel et al., 2017). If the merging process happens within the age of the Universe, then these systems can produce a GW signal.

Studies on the conditions for stable MT to obtain CO mergers have been carried out, which considered the following configuration: a semi-degenerate binary composed of a CO and an arbitrarily evolved donor star (Gallegos-Garcia et al., 2021; Marchant et al., 2021; Picco et al., 2024). This thesis considers the earlier evolution of the CO progenitor. Before the first CO is formed, a previous interaction phase can occur, but this time from the CO progenitor star onto its companion. During this process, the stellar companion will now gain an enriched composition, creating a change in the stellar interior. The stability between the (enriched) donor star and the CO is dependent on both the masses of the components and on their orbital separation, but also crucially, on their stellar structure and therefore will have a direct influence on the final fates of the binary system. Thus, as the title states, in this thesis, we investigate the role of stellar structure on forming merging double compact objects.

In order to study this, we have developed two different methodologies using the stellar evolution code *Modules for Experiments in Stellar Astrophysics*. In Chapter 2, we will not yet include the evolution before the formation of the first BH, but rather imitate the effect of the previous interaction. In the following chapter, we do perform full end-to-end binary evolution simulations. With this, we analyse the change in behaviour of the initial properties of the predicted binary black hole (BH) mergers.

From the results of Chapter 2, it is confirmed that the stability boundary is dependent on the interior structure of the donor star. Doing the full end-to-end binary evolution, we

find a limited set of predicted BH mergers, compared to the results of Chapter 2. This shows that not including the earlier evolution overestimates the stable MT channel. In general, we see that regardless of the donor star experiencing a perturbed composition, there are still semi-degenerate binaries spanning a range of mass ratios and orbital periods able to produce GW signals through stable mass transfer.

Summary for General Audience

Even though we do not see it, many stars in the sky exist in pairs with one or more companions, which scientists call a binary (or multiple) system. There are many scenarios in which these systems can spend their lives with one another, but in this thesis, we will consider the following. Two massive stars with masses higher than eight times the mass of our Sun orbit around each other, each living off of their fuel provided deep in their cores. The more massive one, which we will now call star 1, will tend to age more quickly than its companion, star 2, as it burns through its fuel faster. As star 1 gets older, it will start to expand, and once it is large enough, it will start to shed its outer layers of material and donate them to star 2. Star 2 now has material that used to belong to star 1, changing its structure.

As time goes on, star 1's fuel eventually runs out, and there is no more energy left to sustain its own gravity. Due to its high mass, the gravitational pull is so high that the star will collapse into itself, creating the most compact remnant known in the Universe: a black hole. Of course, star 2 will continue to evolve as well, and it is now their turn to expand and donate its outer layers, but this time to its black hole companion. As mass is being funnelled to the black hole, the distance between the two objects will reduce. At last, star 2 will run out of fuel too, and the binary system will experience a second black hole formation. Due to the orbital shrinkage of the second transfer of material, the two black holes are now circling each other in a very close orbit. In the course of time, these objects will orbit closer and closer to one another, and as they keep on growing closer, they will finally collide.

According to Einstein's theory of General Relativity, this collision can generate ripples that are able to propagate through the fabric of the Universe as fast as the speed of light, called Gravitational Waves. As these waves travel through the cosmos, our detectors are able to hear their echoes and detect properties tied to the signal and its origin. The objective of this thesis will be investigating the success of the above-explained scenario on the special events that are the production of Gravitational Waves. Specifically, we will study the effect of the changed stellar structure of star 2 on the final fate of the binary.

List of Figures

List of Tables

Contents

Chapter 1

Introduction

It has been well-known that the majority of stars exist gravitationally bound with one or more companions, presenting systems known as *binaries* or *multiples*, respectively (Abt & Levy, 1976). Not only are binary stellar systems common in our Universe, they are responsible for some of the most intriguing cosmic phenomena in nature, such as X-ray binaries, radio millisecond pulsars, cataclysmic variables and many more (Tauris & van den Heuvel, 2023). It was the observation of the binary system PSR B1913+16 that led to the positive indication towards the existence of gravitational waves (GW; Hulse and Taylor 1975). The precise match between the decreasing change in the period of this system and its predicted gravitational decay granted the physicists Russell Hulse and Joseph Taylor the 1993 Nobel Prize. It was only in 2015 that gravitational waves (GWs) were directly detected through the joint observatories of LIGO (B. P. Abbott et al., 2016).

Large numbers of gravitational wave observations are expected to take place throughout this and the following decade. The increase of detections are due to new technological advancements for already existing ground-based facilities and due to upcoming future missions. This will provide an abundance of information on gravitational waves physics and the stellar evolution that preceded their formation. Every GW signal observed by the LIGO-Virgo-Kagra (LVK) network after the first detection originates from merging double compact objects, giving a unique method to study their progenitor systems: massive binary stars. Because of this, it is extremely important to provide detailed theoretical models to complement these detections, both to understand the diversity in the current GW data as well as for disentangling the contribution between different evolutionary channels of the GW sources.

This chapter will provide a small introduction to massive star physics - both for single and binary stars - to introduce key concepts on which this thesis is built. We will start with a section on the late stages of massive star evolution, after which we will transition to a more thorough explanation of fundamental properties of (massive) binary systems. This follows up with a segment on gravitational wave astrophysics, including the possible evolutionary pathways that bridge the final fates of the massive binary to their potential GW signal. This chapter finishes with an outline of this thesis.

1.1 Late stages of massive star evolution

The fate of stars is strongly dependent on their initial mass at birth. A star is classified as massive once it can experience core collapse at the end of its lifetime. This can occur when its initial mass is approximately larger than $8\ M_\odot$ (Fryer, 1999). Even though the majority of the Universe is populated with low- and intermediate-mass stars, the higher end of the stellar mass regime offers us a wide variety of topics to study. They are sources of several important astrophysical phenomena, such as their ability to generate radiation-driven winds (Vink, 2022) and cause strong supernovae once they form a sufficiently massive iron core and collapse. Due to this, massive stars are very often described as the cosmic engines of the Universe as they play a critical role in the evolution and chemical enrichment of galaxies (Nomoto et al., 2013). Throughout their evolution, their characteristic feedback processes supplement their environment with heavier metals, which in turn drive the birth of the next generation of stars (Chiosi & Maeder, 1986; Geen et al., 2023).

As this thesis will mainly focus on massive binaries with compact objects (COs), the aim of this section is not to give a thorough overview of massive single stars, but rather to give an introduction to the late evolution leading up to the formation of compact objects and the relevant physics related to this. In this section, we start with a brief part on their pre-supernova evolution and will continue with their end stages as the most compact remnants originating from stars. This section is inspired by Chapters 12 and 13 of the lecture notes on stellar evolution written by Onno Pols and Part VIII on Compact Objects from 'Stellar Structure and Evolution' by Rudolf Kippenhahn, Alfred Weigert and Achim Weiss.

1.1.1 Single star evolution

The birth of a star is defined through the onset of core hydrogen burning into helium, which initiates the long-lived *main sequence* (MS) stage, during which stars evolve on a nuclear timescale. After this process, the star is left with a helium core and it will rapidly readjust as it loses thermal equilibrium without its main energy source. Between core hydrogen depletion and core helium ignition, the stellar core contracts and the hydrogen-rich envelope expands, starting hydrogen shell burning from its inner layers outwards. The star is now a (super) giant. After core helium burning, the same process remains: once the nuclear fuel is depleted in the core, the core will contract while shell burning proceeds. During core contraction, the core temperature increases and once the appropriate temperature is reached, the next burning stage can take over. This process will eventually create concentric layers of products from different nuclear processes. The nuclear burning can continue to heavier elements, with each successive phase more rapid than the one before. For example, for a $15\ M_\odot$ mass star, carbon burning lasts $5\ 000$ years, oxygen burning 1.7 years and the next phase of silicon burning only a few days.

The low- and intermediate-mass counterparts ($M \lesssim 8\ M_\odot$) will reach a point where the core does not reach the necessary temperature to continue its subsequent burning stage. These stars will shed their outer layers through winds, revealing a *white dwarf*. The point at which this happens is dependent on their initial mass. For a more detailed review on the final fates of low- and intermediate-mass stars, we refer to Bressan and Shepherd (2024). Massive stars will be able to reach sufficiently high core temperatures to perform non-degenerate burning, which keeps increasing with every consecutive burning cycle. However, once the star generates an

iron core, the star can no longer produce energy through fusion processes in its core. Without this nuclear burning, the star has no more energy to stay stable. Consequently, the core will proceed to collapse and potentially generate an extremely energetic explosion: a type II or type Ib/c *supernova* (SN).

The end of stellar evolution can result in extreme scenarios. As described above, massive stars can experience a core collapse process into an extremely compact object: a *neutron star* (NS) or a *black hole* (BH). The possibility of generating a supernova explosion and the stellar remnant left behind is still an uncertain field. The nature and explosion mechanism of the compact remnant for single stars is dependent on the initial mass of the star and metallicity (we will follow Heger et al. 2003). Heger et al. (2003) analysed the relation of the masses of their helium core and hydrogen envelope and the effect of wind mass loss (in function of metallicity) on the fates of the remnant for single stars.

For lower sub-solar metallicities, the final helium core mass and hydrogen envelope mass are higher and the star experiences less stellar winds. As the core mass increases, so will the binding energy of the star. For stars with initial masses of $M \lesssim 25\ M_\odot$[1] (and corresponding final core mass of $\sim 8\ M_\odot$), the final remnant will result into a neutron star. They will have more success in generating a SN explosion because they have higher kinetic energies at the point of collapse and a lower binding energy of the outer layers, making it easier to expel them. For the higher initial masses ($\lesssim 40\ M_\odot$ with final core mass over $15\ M_\odot$), the gravitational pull is too high, making the ejected material fall back onto the proto-neutron star, generating a (fallback) BH. For stars with even higher initial masses, the star will not experience this fallback and due to the high gravitational pull, will directly collapse into BH without a SN explosion. For higher solar-like metallicities, the fates will be affected by stellar winds and their lower core and hydrogen envelope masses, resulting in different scenarios (see Fig. 1 of Heger et al. 2003).

1.2 Massive binary star evolution

Since the stars are gravitationally bound to one another, their orbital motion can reveal certain properties that we are not able to constrain from single stars only. There are several complementary observational techniques to analyse binary systems (for a full review on 'Observing Binaries', see Sana and Vrancken 2025). For relatively long binary separations, it is more suitable to consider interferometry or even high-contrast imaging techniques, which are able to resolve the individual binary components. For short period binaries, we use photometry or spectroscopy. Spectroscopy uses the concept of the Doppler effect to detect shifts in the spectral lines, from which we can calculate changes in the line-of-sight radial velocities (RV). With eclipsing binaries (where one star passes in front of the other, depending on the geometry w.r.t the observer), variations in light flux can be detected. Depending on the science objective, one observation technique is more beneficial than the other, or an interplay of different methods could be necessary.

It has long been known that many stars belong in binaries (Abt & Levy, 1976), indicating that binarity is of great importance to stellar populations. However, it is through the last

[1]Note that these numbers are still uncertain and that we take values from Fryer (1999).

decade that it has been well established that binary evolution shapes the lives of massive stars. Dedicated spectroscopy and additional complementary techniques such as the ones described above have proven that the majority of massive stars exist in close binaries coupled with careful consideration of observational biases (Sana et al., 2012). They will experience interaction between the two components at some point in their evolution. The most prominent source of interaction in binaries is through *mass transfer* (MT), which can dramatically alter the evolution of both binary components, resulting in different end products compared to single star evolution.

An important early mention of mass transfer originates from the *Algol paradox*. In the 1950s, an interesting eclipsing binary was found with an unevolved more massive component with a less massive but further evolved subgiant companion. This configuration was thought unusual considering stellar evolution dictates that more massive stars are expected to evolve faster than stars with smaller masses. It was Crawford (1955) who suggested that the less massive subgiant could have been the initially more massive and that the change in mass can be explained by substantial mass transfer from the subgiant to the less evolved star.

In the following sections, we will cover how mass transfer affects the binary and its orbit and the role of mass transfer stability. Most of the following content is based on Marchant and Bodensteiner (2024), Chapters 6 to 8 from the lecture notes of Onno Pols on 'Binary Stars' and Chapter 4 of Tauris and van den Heuvel (2023).

1.2.1 Roche lobe overflow

In binary systems, the concept of the Roche potential refers to the effective potential (both gravitational and centrifugal) in the co-rotating frame of a circular orbit. The local minimum of this potential between the two stars marks the position of the first Lagrangian point L_1. The critical equipotential surface crossing L_1 defines the two volumes around each star as the Roche lobes (see Fig. 1.1). We can make use of the radius equivalent with the radius

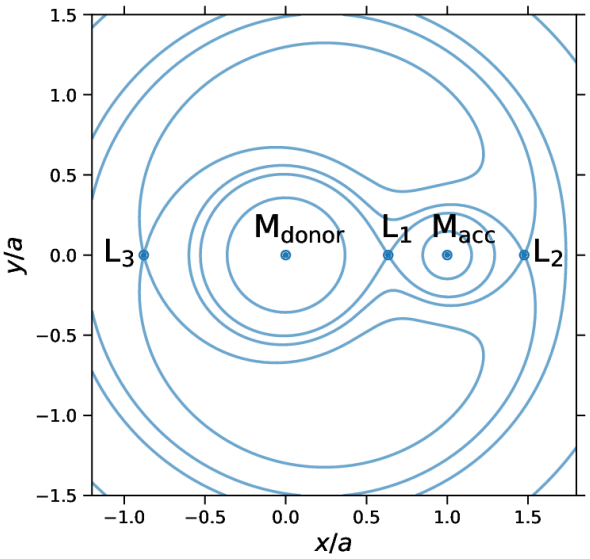

Figure 1.1: Contours of the equipotential surfaces for a binary system with $m_{\rm d} = 5.0\ M_\odot$ and $m_{\rm a} = 1.3\ M_\odot$, which indicates the first three Lagrangian points. After Misra et al. (2020).

of a sphere with the same volume as the Roche Lobe to measure the size of the star ($R_{\rm RL}$). As there is no analytical expression for $R_{\rm RL}$, we can instead consider a numerical fit done by Eggleton (1983). This approximation considers the radius of the primary star $R_{\rm RL,1}$ with the mass ratio ($q = m_2/m_1$) and orbital separation a:

$$\frac{R_{\rm RL,1}}{a} = \frac{0.49q^{-2/3}}{0.6q^{-2/3} + \ln(1 + q^{-1/3})}. \tag{1.1}$$

We compare the radius of the star to that of the Roche lobe radius to indicate when the star is large enough to start the mass transfer. In the case where the radius of the star exceeds the Roche lobe radius, the outer layers of the star can no longer remain in hydrostatic equilibrium and will transfer mass through the first Lagrangian point L_1 into the Roche lobe of its companion. This process is called *Roche lobe overflow* (RLOF).

In terms of the Roche potential, one can distinguish the three different equilibrium configurations in which the binary can exist (see Fig. 1.2). In a *detached binary*, the radii of both stars are smaller than their Roche lobe radius, meaning that their surfaces match an equipotential surface that is still inside the Roche lobes. If one of the stars fills their Roche lobe while their companion does not, we classify the binary as *semi-detached*. The system experiences RLOF. Lastly, if both stars fill an equipotential surface exceeding the potential of their Roche lobes at L_1, we have a *contact binary*.

In addition to this classification, consider also the classification scheme for interacting binaries as defined by Kippenhahn and Weigert (1967), which flags different evolutionary phases of the donor star at the onset of RLOF. If the interaction starts during the main sequence, we have *Case A* mass transfer. If the mass transfer initiates between the main sequence and core helium depletion, we classify the episode as *Case B* mass transfer and lastly, if the interaction starts after core helium depletion, we have *Case C* mass transfer (Lauterborn, 1970).

Orbital evolution

When a system experiences RLOF, mass transfer alters both the orbit and the structure of the stars. The expression for orbital angular momentum $J_{\rm orb}$ in function of the binary separation a and the component masses m_1 and m_2, assuming a circular orbit ($e = 0$) is

$$J_{orb} = m_1 m_2 \sqrt{\frac{Ga}{m_1 + m_2}}. \tag{1.2}$$

Differentiating this expression results in

$$2\frac{\dot{J}_{\rm orb}}{J_{\rm orb}} = \frac{\dot{a}}{a} + 2\frac{\dot{m}_1}{m_1} + 2\frac{\dot{m}_2}{m_2} - \frac{\dot{m}_1 + \dot{m}_2}{m_1 + m_2}, \tag{1.3}$$

which describes the responding change in angular momentum as the component masses and binary separation change due to the mass loss of one of the individual components. The above assumption of a circular orbit is often justified since tidal interactions within a semi-detached binary can decrease the eccentricity e on timescales significantly shorter the nuclear timescale (Verbunt & Phinney, 1995). However, it is important to state that there are some cases where tides are not efficient to circularise the binary (e.g. Rocha et al. 2025). RLOF will further

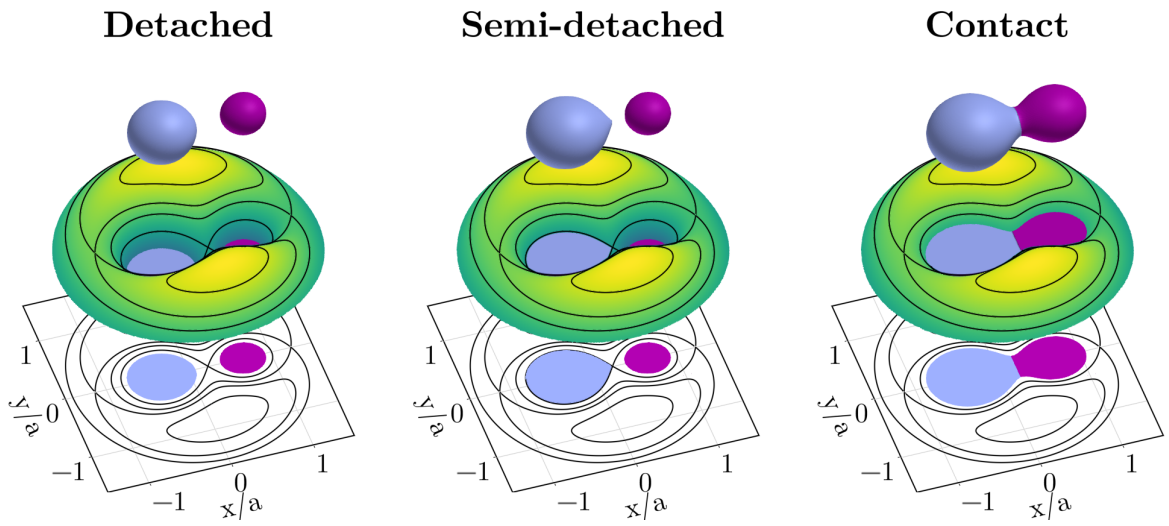

Figure 1.2: A schematic overview of a detached, a semi-detached and a contact binary for a system with $q = 0.5$. *Lower:* The contours of the equipotential surfaces in the xy-plane. *Middle:* 3D shapes of the values of potential in the xy-plane reflected in the z-direction in arbitrary units. *Upper:* 3D shapes of both stellar components. Adapted from Marchant (2025).

decrease the eccentricity, circularising the pre-RLOF orbit (Sepinsky et al., 2010). The angular momentum of this described system can be influenced by several physical effects. Consider the different components that can affect the orbital angular momentum:

$$\frac{\dot{J}_{\rm orb}}{J_{\rm orb}} = \frac{\dot{J}_{\rm GW}}{J_{\rm orb}} + \frac{\dot{J}_{\rm mb}}{J_{\rm orb}} + \frac{\dot{J}_{\rm ls}}{J_{\rm orb}} + \frac{\dot{J}_{\rm ml}}{J_{\rm orb}}. \tag{1.4}$$

The first term on the right-hand side of Eq. 1.4 refers to the orbital effects due to the emission of gravitational waves (Peters, 1964). The second term describes the change in orbital momentum from *magnetic braking* (Schatzman, 1962; Mestel, 1968). This effect is only applicable to objects with high magnetic activity. This thesis will focus on the evolution of early-type stars, where magnetic braking is not expected to play a role. Tidal orbit-spin coupling effects can take place between the angular momentum of the orbit and the spin of the individual objects ($\dot{J}_{\rm ls}$). However, for the following sections we will only consider the last fourth term, which encapsulates the changes in angular momentum through mass transfer processes. Several approximations can describe the orbital changes originating from mass loss or mass transfer, with each having different corresponding 'modes'. We will focus on *conservative mass transfer* and mass transfer described by *isotropic re-emission*. For a further detailed explanation of orbital effects due to mass transfer and/or mass loss in binary systems, we refer to Soberman et al. (1997), van den Heuvel et al. (2017) and Tauris and van den Heuvel (2023).

Consider the constraints where both the orbital angular momentum ($\dot{J}_{\rm orb} = 0$) and total mass ($\dot{m}_1 + \dot{m}_2 = 0$) of the binary system is conserved. Even though there is no mass escaping the total binary system, the orbital separation can still change if there is a mass exchange between the components. We can now rewrite Eq. 1.3, but since we are referring to mass exchange between the components, we will now change the subscripts of the masses from m_1 and m_2 to $m_{\rm d}$ and $m_{\rm a}$ to refer to the donor and accretor instead of primary and secondary

component.

$$\frac{\dot{a}}{a} = 2\frac{\dot{m}_d}{m_\mathrm{d}} + 2\frac{\dot{m}_a}{m_\mathrm{a}} = 2\left(\frac{m_\mathrm{d}}{m_\mathrm{a}} - 1\right)\frac{\dot{m}_d}{m_\mathrm{d}} \tag{1.5}$$

This last relation states that since the donor star is losing mass ($\dot{m}_\mathrm{d} < 0$), the binary separation will shrink ($\dot{a} < 0$) as long as the donor mass stays larger than the accretor mass ($m_\mathrm{d} > m_\mathrm{a}$). In the limit of $m_\mathrm{d}/m_\mathrm{a} \to \infty$, we see from Eq. 1.5 that $\dot{a}/a \to \infty$, indicating that the orbital contraction becomes more extreme for mass ratios away from unity. Once the mass ratio is inverted during mass transfer ($m_\mathrm{d} < m_\mathrm{a}$), the orbit will consequently widen ($\dot{a} > 0$). We can rewrite Eq. 1.5 to an explicit relation between the orbital separation and the mass ratio ($q = m_\mathrm{a}/m_\mathrm{d}$) in terms of the initial separation a_i and initial mass ratio q_i as

$$\frac{a}{a_\mathrm{i}} = \left(\frac{q_\mathrm{i}}{q}\right)^2 \left(\frac{q+1}{q_\mathrm{i}+1}\right)^4 \tag{1.6}$$

or, by using Kepler's third law ($P^2 \propto a^3/m$), we can rewrite this in terms of period (and initial period P_i) instead of orbital separation

$$\frac{P}{P_\mathrm{i}} = \left(\frac{q_\mathrm{i}}{q}\right)^3 \left(\frac{q+1}{q_\mathrm{i}+1}\right)^6. \tag{1.7}$$

Isotropic re-emission and the Eddington limit

Even though multiple post-interaction systems seem to indicate that they experienced (mostly) conservative mass transfer (Lechien et al., 2025), the idea that angular momentum and total mass stay conserved does not always hold. Up until this point, we have not yet specified the components of the binary when discussing the interaction processes. However, for the remainder of this section, we will consider a binary with a star plus compact object (CO) configuration and examine the physics of mass transfer from the donor star accreted onto the compact object. The model of isotropic re-emission describes this situation where a fraction of the transferred mass (β) onto the CO will get ejected (see artistic impression in Fig. 1.3). The ejected material will carry the specific angular momentum from the CO accretor out of the system.

A CO that is accreting mass from its companion will experience a physical limit on the accretion luminosity where further accretion will be prevented. This limit is described by the *Eddington luminosity* (L_Edd), which provides an upper limit for the accretion luminosity (L_acc) from a spherically accreting CO. The Eddington luminosity can be derived from equating the outward force originating from the radiation pressure of the plasma near the surface to the inward gravitational force (see full derivation in Tauris and van den Heuvel 2023). By doing this and rewriting some fundamental physical properties, we get the following expression using the *mean opacity* κ ($\mathrm{cm^2\ g^{-1}}$), M being the mass of the CO, G the gravitational constant and c the speed of light:

$$L_\mathrm{Edd} = \frac{4\pi GMc}{\kappa} \simeq \frac{4\pi GMc}{0.2(1+X)}. \tag{1.8}$$

In the last step, we have simplified the mean opacity in terms of the hydrogen mass fraction X. If we consider a hydrogen-rich donor star with $X = 0.70$ and with a mass of $30\ M_\odot$, the Eddington luminosity would yield a value of $L_\mathrm{Edd} = 4.5 \times 10^{39}\ \mathrm{erg\ s^{-1}}$. For a described system

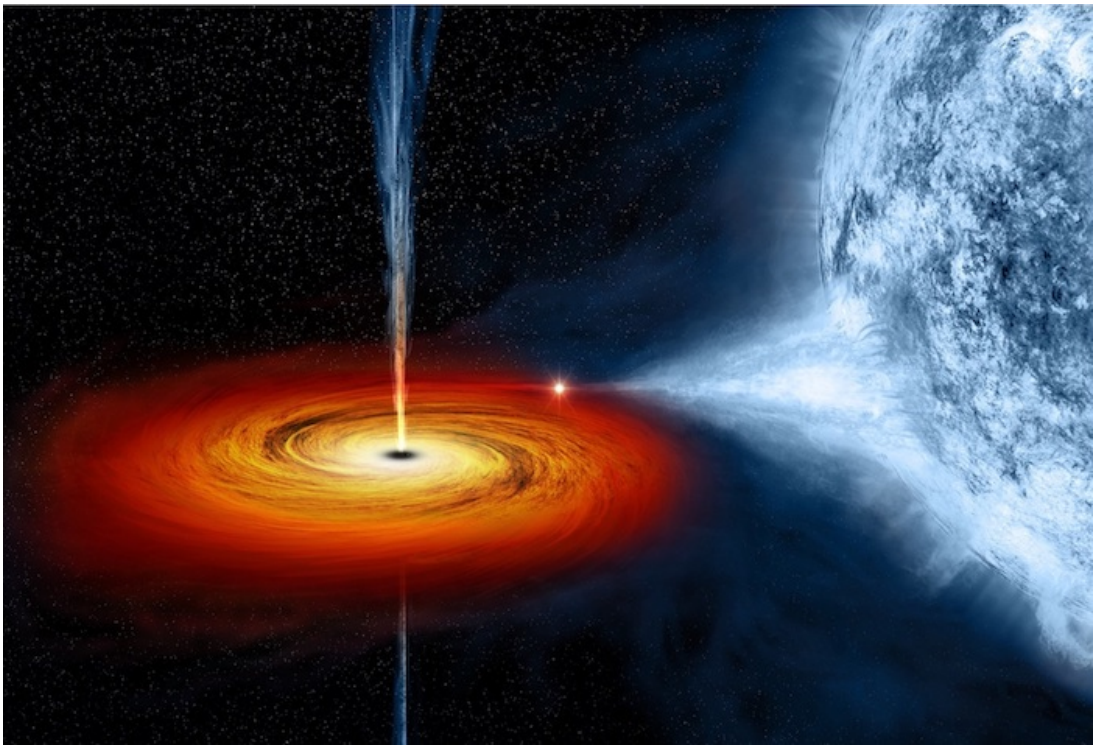

Figure 1.3: An artistic impression of a high-mass X-ray binary showing an example of mass getting partially accreted and partially ejected. Credits: NASA/CMC/M.Weiss.

where mass gets accreted onto a CO through mass transfer, we can use the above expression to define the Eddington mass accretion rate. We use $L = \epsilon \dot{M}$, with $\epsilon = \epsilon_{\rm grav} + \epsilon_{\rm nuc}$ $(\mathrm{erg\ g^{-1}})$, where we have defined the gravitational energy released from the accreting matter $\epsilon_{\rm grav}$ and the nuclear energy $\epsilon_{\rm nuc}$ from burning processes at the surface edge of the CO:

$$\dot{M}_{\rm Edd} = \frac{4\pi G M c}{\kappa \epsilon}. \tag{1.9}$$

For disk accretion onto a BH, ϵ will correspond to a significant fraction of the rest mass energy ($\epsilon/c^2 \simeq 0.06 - 0.42$, depending on the spin Bardeen et al. 1972). Because of this, the massive donors companion of BHs can often exceed the Eddington luminosity by several orders of magnitude. Consider again the isotropic re-emission model with a fraction β of transferred mass getting ejected rather than accreted. To not exceed the Eddington limit, certain star+CO binary systems will undergo isotropic re-emission, where the majority of the accreted matter will be expelled due to the radiation pressure. We can produce a similar expression to Eq. 1.7 for the isotropic re-emission model in the limit where all mass is ejected, or $\beta \to 1$ (see Tauris and van den Heuvel (2023) for detailed derivations and also King et al. 2001):

$$\lim_{\beta \to 1} \left(\frac{P}{P_{\rm i}} \right) = \left(\frac{q_{\rm i}}{q} \right)^3 \left(\frac{q_{\rm i} + 1}{q + 1} \right)^2 e^{3(q - q_{\rm i})}. \tag{1.10}$$

This is also referred to as a *fully non-conservative* limit of isotropic re-emission. As shown in, e.g., Marchant (2025), fully non-conservative isotropic re-emission can reach notably smaller orbital separations than the conservative limit for initial mass ratios of $q_{\rm i} = m_{\rm a,i}/m_{\rm d,i} < 1$.

1.2.2 Mass transfer stability

The stability and evolutionary outcomes of the mass transfer process depend on the response of: the radius of the donor star due to mass loss, the orbit (and thus $R_{\rm RL}$) due to mass transfer and lastly, the accretor. In the following description of mass transfer stability, we will assume the donor to be transferring mass onto a point mass. This allows us to discuss the reaction of the donor star and orbit only. With this, we will explore the *stability criteria* by comparing the radius of the donor star to the Roche lobe radius as a function of donor mass. We can express the above-mentioned mass-radius relation with the following exponents. They represent the adiabatic response of the donor radius and the change of the Roche lobe radius $R_{\rm RL}$ as mass changes (by e. g. transferring mass; Soberman et al. 1997).

$$\zeta_{\rm ad} = \left(\frac{d\log R_{\rm d}}{d\log M}\right)_{\rm ad}, \ \zeta_{\rm RL} = \left(\frac{d\log R_{\rm RL}}{d\log M}\right) \tag{1.11}$$

When a star loses a fraction of its mass, the layers underneath that of the transferred mass will lose inward pressure. Therefore, the radius of the star will readjust to retain hydrostatic equilibrium. We classify mass transfer as *dynamically stable* if $\zeta_{\rm ad} \geq \zeta_{\rm RL}$, since mass transfer will not lead to ever-increasing mass transfer rates. In this case, the radius of the donor star is able to adjust to the mass transfer while remaining in hydrostatic equilibrium.

If mass transfer is dynamically stable, one has to consider if the star remains in thermal equilibrium during the mass transfer process. We can introduce another exponent $\zeta_{\rm eq}$, which can be written as:

$$\zeta_{\rm eq} = \left(\frac{d\log R_{\rm d}}{d\log M}\right)_{\rm eq}. \tag{1.12}$$

This describes the change in the thermal equilibrium radius $(\delta R/R_{\rm d})_{\rm eq}$ that the donor wants to achieve as it is responding to its new mass $M_{\rm d} + \delta M_{\rm d}$ ($\delta M_{\rm d} < 0$). This introduces a stricter constraint for *secularly stable* mass transfer where both $\zeta_{\rm ad} \geq \zeta_{\rm RL}$ and $\zeta_{\rm eq} \geq \zeta_{\rm RL}$ must be reached. The donor star remains both in hydrostatic and thermal equilibrium during the mass transfer. We expect the mass transfer to happen on the nuclear timescale. For the intermediate case where $\zeta_{\rm ad} \geq \zeta_{\rm RL} > \zeta_{\rm eq}$, the mass transfer is driven by the thermal re-adjustment of the donor star and the mass transfer is happening on a thermal timescale. Note that in the above description, we assume the donor star to be in thermal equilibrium before filling the Roche lobe.

The opposite situation where $\zeta_{\rm RL} > \zeta_{\rm ad}$ can occur in nature as well. In this case, the adiabatic response is not sufficient for the donor to stay within its Roche lobe, resulting in an *unstable* mass transfer process that will lead to escalating mass transfer rates. Both stable and unstable mass transfer can alter the evolution of both components and their orbit significantly. In the unstable case, the system experiences a *common envelope* (CE) evolution (Paczynski, 1976). Then, the outer material that the donor is transferring will eventually engulf its companion, creating a common environment for both objects. Two major outcomes can result from the CE evolution. In the first scenario, the loss of angular momentum leads to the objects spiralling in within the common envelope, after which the system will produce a stellar merger. In the second scenario, the system ejects its common envelope from the released gravitational energy and angular momentum originating from the spiral inwards.

1.3 Gravitational wave astronomy

In the theory of General Relativity, Gravitational Waves (GWs) are defined as ripples propagating through the medium of space-time at the speed of light (Einstein, 1915). As these waves travel through the Universe, they can carry information about their signal and origin. The first observational evidence of the existence of gravitational radiation was the Hulse-Taylor pulsar, observed in 1974 (Hulse & Taylor, 1975). This discovery showed a pair consisting of a neutron star and a pulsar with a decaying change in period that was in agreement with the one caused by the release of gravitational radiation as general relativity predicted. The first direct detection of a gravitational wave signal was not found until recently, when the joint detectors of the advanced Laser Interferometer Gravitational wave Observation (aLIGO), housed at the outskirts of the United States of America, observed a signal inferred to be the source by the coalescence of two black holes in 2015 (B. P. Abbott et al., 2016).

In the following sections, we will take a closer look at GW detectors and their development, as well as certain information carried by the GW signals from merging COs. In addition to this, we end this section by going through the evolutionary channels that can produce a GW source. The following subsections are based on Mandel and Farmer (2022) and Marchant and Bodensteiner (2024).

1.3.1 Gravitational wave detections

After a successful fourth observational run, we are currently officially at approximately one hundred observations of gravitational wave signals detected by ground-based observatories. These observations are compiled into the *Gravitational Wave Transient Catalogues* (GWTCs) made possible by the LIGO-Virgo-Kagra (LVK) collaboration (R. Abbott et al., 2023). All present observations of the first three observational runs are inferred to originate from compact object coalescences of either NSs or BHs.

The current sample of gravitational wave detections will steadily grow due to the continuous improvement of the current GW detectors, expecting over a thousand detections by the end of the decade (see Fig. 1.4; Broekgaarden et al. 2024). Furthermore, this number will grow even more with the next generation of GW observatories. The *Einstein Telescope* (ET) will offer a new range of possibilities due to its wider frequency band and its order of magnitude increase in sensitivity (Maggiore et al., 2020). Another important effort to mention is the *Laser Interferometer Space Antenna* (LISA; Amaro-Seoane et al. 2017), which will be capable of reaching the mHz frequency range of inspiralling white dwarfs. By using spacecrafts, LISA can tackle the obstacle of seismic noise that the ground-based detectors encounter. Another method to indirectly detect the effect of gravitational radiation is through millisecond pulsars. The *International Pulsar Timing Array* (iPTA; Manchester and IPTA 2013) observes the ultra-low frequency window (probing supermassive black hole binaries) by detecting and characterising the time of arrival of the signals of radio millisecond pulsars.

Each detector has its own signature sensitivity band in which it operates, each covering a specific frequency range. The characteristic (dimensionless) strain $h = \delta L/L$ is defined as the deviation in length caused by the GWs across a detector. The strain sensitivity curves of several GW detectors are shown in Fig. 1.5. Relevant information that can be extracted from

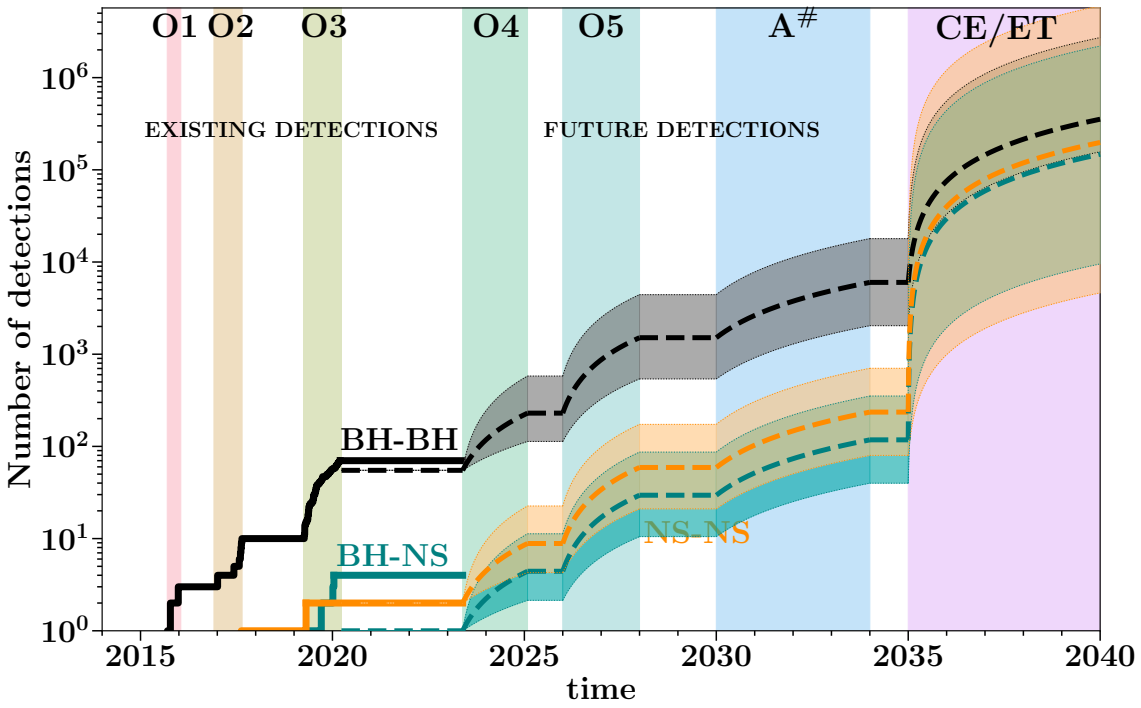

Figure 1.4: The expected number of future merger detections from BH+BH systems (black), BH+NS systems (teal) and NS+NS systems (orange). Labels on the top of the figure indicates the existing and future observational runs (O1, O2, O3, O4 and O5) from the LVK collaboration. A# indicates the future best sensitivity of the LIGO/Virgo detectors and CE/ET represents the era of the Cosmic Explorer (CE; Hall 2022) and the Einstein Telescope (ET). From Broekgaarden et al. (2024).

the GW catalogue is the *chirp mass*, the *mass ratio* and the *effective spin*:

$$\mathcal{M} = \frac{(m_1 m_2)^{3/5}}{(m_1 + m_2)^{1/5}}, \quad q = \frac{m_2}{m_1} \quad \text{and} \quad \chi_{\text{eff}} = \frac{m_1\chi_1 + m_2\chi_2}{m_1 + m_2}. \tag{1.13}$$

In the above expressions, we use the respective masses m_1 and m_2 and the respective components of the spin aligned with the orbital momentum χ_1 and χ_2 of the two compact objects. It is important to state that the GW catalogue defines the mass ratio to be lower than zero (lower mass over higher mass).

1.3.2 Evolutionary channels

All inferred sources of gravitational waves (from the first, second and third observational runs) originate from merging double compact objects. In order to produce a scenario that would lead up to a CO merger, we have to consider the following challenges. On one hand, the double COs will have to exist in a tight orbit to be able to inspiral within the age of the Universe (13.8 Gyr) to produce a successful CO merger. For a circular binary, the time it takes for the binary with component masses m_1 and m_2 at a certain initial separation a_0 to evolve to a merger is expressed as

$$t_{\text{merger}}(a_0) = \frac{a_0^4}{4\beta} \quad \text{with} \quad \beta \equiv \frac{64}{5}\frac{G^3 m_1 m_2 (m_1 + m_2)}{c^5} \tag{1.14}$$

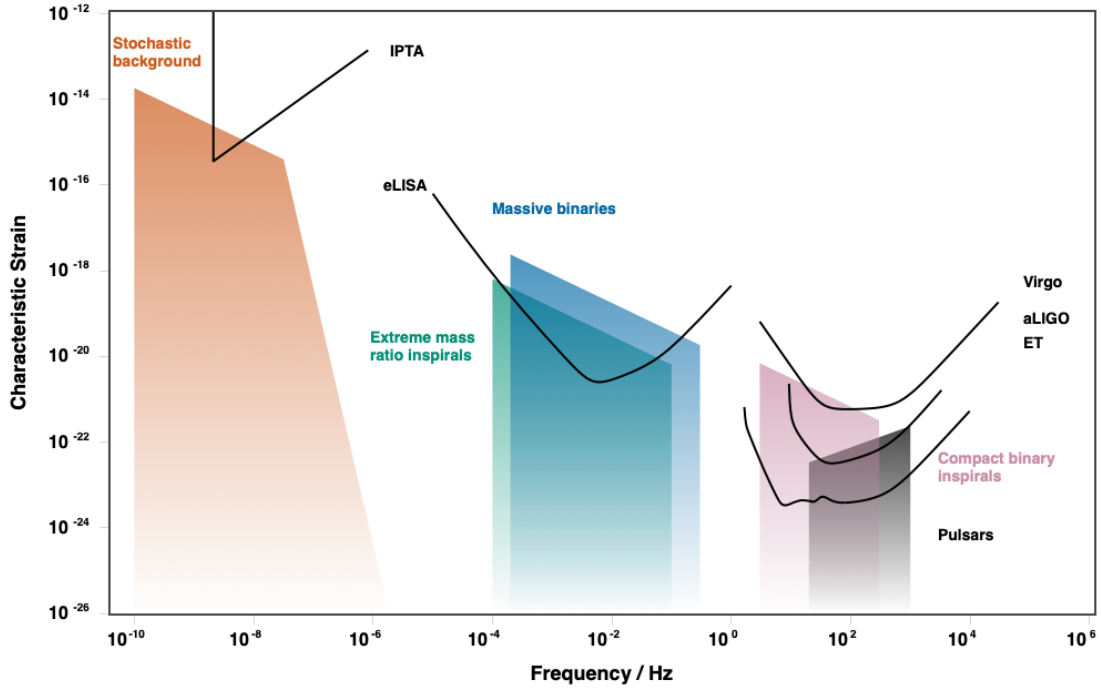

Figure 1.5: The characteristic strain of the indicated detectors versus frequency. This image was made with the virtual *Gravitational Wave Sensitivity Curve Plotter:* `http://www.sr.bham.ac.uk/cplb/GWplotter/` (Moore et al., 2015)

On the other hand, as stars evolve, they will start to expand as (super)giants. In case of a very short period binary, they can produce a stellar merger before they have the possibility of evolving into a BH or NS. Therefore, in order to fit both stars in a binary orbit after the expansion, the initial separation would have to be large. The objects are then too far apart in order to be able to merge within the age of the Universe, implying that merging COs formed through binary evolution must include strong interaction processes. There have been multiple formation channels[2] put forward to explain the binary evolution leading up to gravitational waves. The contribution of each of the formation channels to the observed sample is still an open question in the field. However, it has been suggested through comparison between theoretical distribution and observations that we have to consider an interplay of processes (Zevin et al., 2021). It is important to stress that regardless of the formation channel that the CO binary[3] experienced, a CO merger is a rare phenomenon.

From the multiple formation channels, there are several that do not necessarily involve binary evolution processes. Consider the channel described through *dynamical processes* in clusters (Kulkarni et al., 1993; Sigurdsson & Hernquist, 1993; Portegies Zwart & McMillan, 2000; Rodriguez et al., 2015; Di Carlo et al., 2019; Mapelli, 2021). Inside a dense globular cluster, black holes (either single or inside a binary) tend to migrate towards the centre of the cluster. Through many body interactions, stars inside binaries can be exchanged with these black holes

[2]For a recent overview summarising the different evolutionary pathways, see Mandel and Farmer (2022).

[3]Note that when we refer to CO binaries, we consider BH+BH, BH+NS or NS+NS binaries, since the scope of this thesis is limited to massive binary stars.

and produce BH binaries. Through subsequent scattering events with another third object, this BH binary can tighten its orbit via energy release to said third object. The close BH binary can experience a recoil kick from its last scattering event and can merge outside of the cluster after this ejection.

Another formation channel suggestion considers inspiralling stellar mass BHs embedded in the gaseous disk of supermassive black holes at the centre of active galactic nuclei (AGNs) (McKernan et al., 2014; Bartos et al., 2017; Stone et al., 2017). It has also been suggested that primordial black holes (PBHs) could form binary pairs via gravitational capture in the early universe that provide detectable merger events in the current epoch (Bird et al., 2016; Sasaki et al., 2018). Regardless of these channels, we will mainly focus on the evolutionary pathways to tight CO+CO systems in isolated binaries (free of n-body interactions).

Isolated binaries

In isolated binaries, the formation channels to the formation of a CO+CO binary invoke either a process that avoids the expansion of the stars or a mechanism that shrinks the orbit. We will concentrate on the formation of the CO+CO binary, where the components would have to experience MT during their star+CO stage that tightens the orbit. However, we will address two formation channels proposed without invoking mass transfer as well.

A methodology to let the binary survive until the formation of COs by preventing the stars from expanding is *chemically homogeneous evolution* (Mandel & de Mink, 2016; Marchant et al., 2016). Consider a massive binary system in a tight orbit such that it can potentially experience a contact phase (see Fig. 1.2). If the separation is sufficiently small, these stars can become tidally locked and consequently increase their respective spin, generating rapidly rotating stars. This rapid rotation, in turn, has a direct impact on the internal chemical mixing of the stars, smoothing out the chemical gradients (Maeder, 1987). Once practically all hydrogen is depleted, the star will contract rather than expand and thus avoid interaction. It has been shown that for metal-poor stars, this process is able to generate a tight CO binary without the need for mass transfer (Marchant et al., 2016). Another channel considers *population III stars*. Due to the lack of metals, the stars are able to have smaller stellar radii and consequently survive in tighter orbits more easily (Belczynski et al., 2004; Kinugawa et al., 2014; Inayoshi et al., 2017).

Consider the two following orbital tightening mechanisms that can occur in isolated binaries: common envelope (CE) evolution (Paczynski, 1976) and stable mass transfer (MT) through Roche Lobe overflow (van den Heuvel et al., 2017). Fig. 1.6 shows two possible pathways of forming merging double COs through either stable MT (path a) or CE evolution (path b)[4]. We start the binary evolutions with two stars at ZAMS (stage 1 in Fig. 1.6). In this example, for simplicity, the first mass transfer episode (stage 2) is indicated as stable mass transfer. This process strips the most massive star of its hydrogen-rich envelope and at the same time changes the composition of its companion. After the first MT, the system consists of a stripped star and a star with an enriched composition (stage 3).

The stripped star evolves further into a compact object (stage 4) and the system can experience the second mass transfer phase (stage 5). The accretor of the first interaction is now the

[4]To see the complete set of binary evolutions, see Chen et al. (2024).

donor, transferring mass onto the compact object, once the radius of the donor star reaches the Roche Lobe radius. On the one hand, in the stable MT channel (stage 5a) proposed by van den Heuvel et al. (2017), the system's orbit can be reduced considerably and could make the formation of double compact objects that will inspiral within the age of the Universe possible. This depends on the mass ratio, period, properties of the (enriched) donor star and mass transfer efficiency. On the other hand, in the CE channel, the second MT episode is unstable (stage 5b). If the system survives the common envelope phase (i.e., envelope ejection), this can result in a star+CO binary that can develop into a merging CO binary (e.g., Belczynski et al. 2016).

1.4 Context & Thesis outline

It has been proposed that non-conservative stable mass transfer between the Roche lobe overflowing star and a CO can tighten the orbit of the star+CO system in favour of the formation of merging double COs (van den Heuvel et al., 2017; Neijssel et al., 2019; Bavera et al., 2021). Neijssel et al. (2019) and Bavera et al. (2021) have shown that compared to the observational sample of GW sources (within uncertainties in various single and binary star processes), the contribution of non-conservative stable MT appears to be larger than the CE channel. Additionally, large uncertainties are present in binary models regarding the CE channel. Since population synthesis studies are crucial to understanding the evolutionary channels of merging binary COs, it is important to state the caveats of their assumptions. Several population synthesis codes assume a direct link between a specific evolutionary stage at the onset of CE evolution and CE survival (Belczynski et al., 2010). This research suggests that interaction after core-helium ignition assures CE survival, while a system that interacts before the onset of core-helium ignition evolves into a stellar merger during CE evolution. However, studies like Marchant et al. 2021 and Klencki et al. 2021 using detailed stellar evolution models report that this method overestimates the CE channel. Considering the above-stated arguments in favour of non-conservative stable mass transfer for merging CO binaries, it is therefore important to study and question its potential.

Recent studies show that the stable MT channel can produce merging double compact objects within the age of the Universe for a broad range of initial parameters (Gallegos-Garcia et al., 2021; Marchant et al., 2021; Picco et al., 2024). However, these papers consider the initial configuration of a binary composed of a CO and a donor star at zero-age main sequence. By implementing this approach, the history of the binary prior to the formation of the first CO is neglected. Therefore, the influence of the donor star composition being perturbed by previous interaction is not accounted for (see stage 2 in Fig. 1.6). The main objective of this thesis is to investigate the effect of an enriched composition of the donor star due to the first MT episode on the success of the stable MT channel to produce merging binary COs (within the age of the Universe).

To do so, we create a large grid(s) of models using the open-source stellar evolution code `MESA` (*Modules for Experiments in Stellar Astrophysics*; Paxton et al. 2011). In these grids, we investigate different initial configurations of the binary system, namely by varying the initial component masses (and thus, the initial mass ratio) and the initial orbital period. In Chapter 2, we adopt a similar methodology described in Marchant et al. (2021), starting the `MESA`

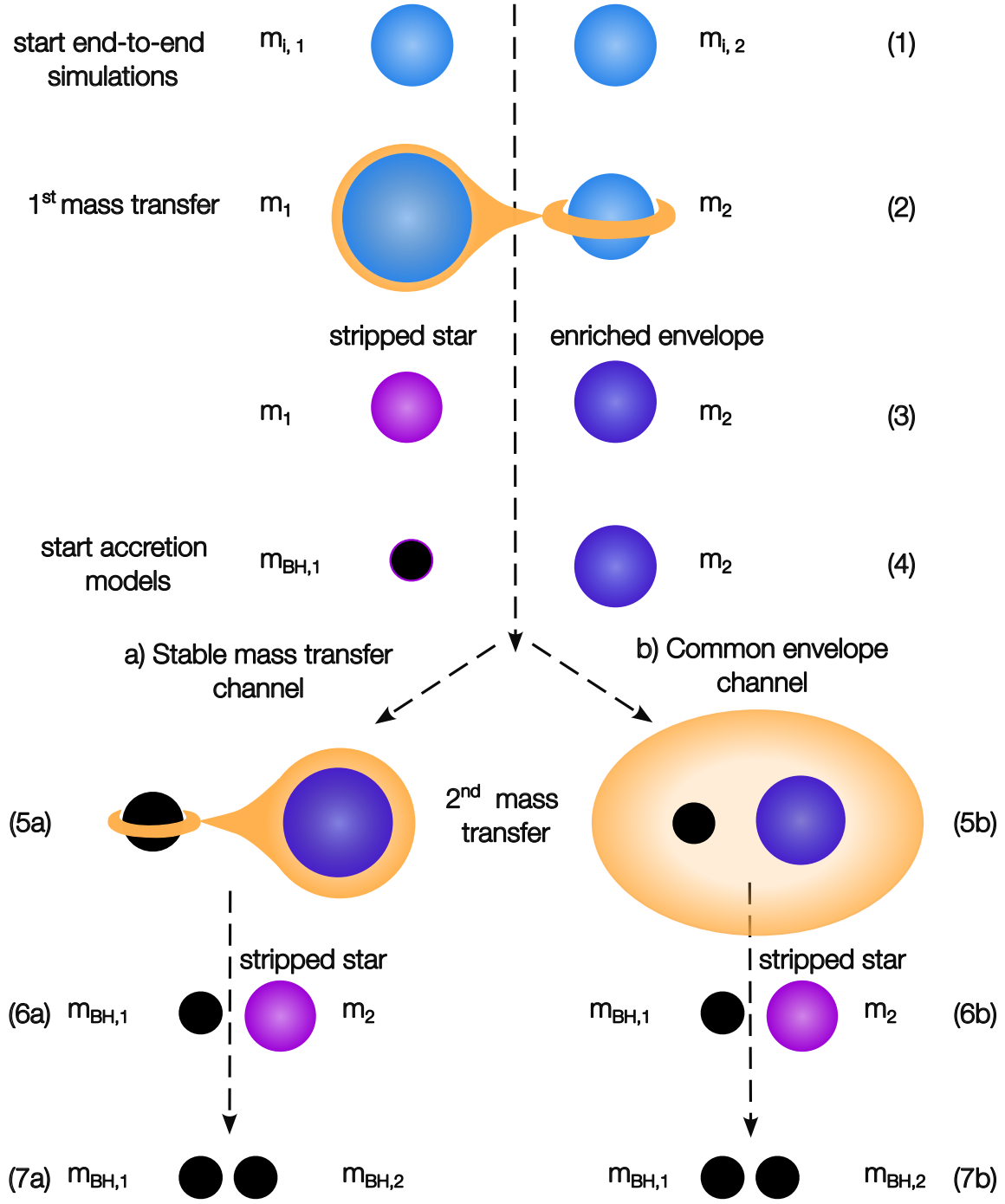

Figure 1.6: Schematic overview of binary star evolutionary pathways that form double compact objects (not to scale). Numbers next to the binary pictograms represent each individual evolutionary stage. Inspired by Fig. 1 from Schneider et al. (2023).

simulations with a donor star+CO configuration (stage 4). Instead of initialising the donor star at ZAMS, we use a model of a star with a perturbed composition. In these model, we mimic the initial mass transfer episode by letting the star experience an artificial accretion process. We consider two accretion models in this chapter, namely one where the accreted

matter composition is hydrogen-rich and one where this is helium-rich. In Chapter 3, we will perform a grid of end-to-end models starting with both stars at ZAMS (stage 1). With these models, we can investigate the robustness of the methodology of Chapter 2 and question the arbitrary a priori assumptions that were made. In the last chapter, we present a sample of observed star+CO systems and provide conclusions and a discussion on the content of the prior two chapters, as well as some future developments that can be done with this research.

Chapter 2

Accretion models

The first method performed in this thesis to investigate the influence of the stellar structure on the conditions of forming black hole (BH) mergers through stable mass transfer (MT) is what we will call the *accretion models*. In this chapter, we will expand on the initial binary configuration as described in Marchant et al. (2021) and Picco et al. (2024): a semi-degenerate binary consisting of a zero-age main sequence (ZAMS) donor star and a BH. We want to account for the mass transfer process before the formation of this BH (stage 2 in Fig. 1.6) since it will enrich the composition of the donor star in this configuration. Due to this enrichment, the donor star will achieve a different composition profile compared to a single star with the same mass. For this reason, we will not initialise this donor star as a ZAMS star, but we will instead use as a starting point a model of a star with a composition perturbed through an artificial accretion process. Thus, we start the simulations with the enriched-star+BH configuration (stage 4). In order to achieve a star with an enriched composition, we will perform a controlled experiment where we let this star accrete material on top of its surface.

A caveat to state is that to properly report on the effect of a prior mass transfer episode, one would have to initiate the binary models at the start of binary evolution with two ZAMS stars (stage 1), which will be done the Chapter 3. However, the approach of the accretion models does offer us many advantages. By starting the simulations at this evolutionary stage (after the formation first BH; stage 4), we reduce the computational cost in comparison to the simulations starting with two ZAMS stars. Aside from this, we can manipulate the physical accretion process happening to the donor star. This reaps the benefit that we can construct accretion models of an arbitrary mass and directly study how the stability is affected compared to the ZAMS+BH models in literature (Marchant et al., 2021). This can not be achieved in the ZAMS+ZAMS simulations of Chapter 3 since we can not modify the final mass of the star that experienced the accretion process. In this chapter, we will produce two different accretion models with a specific mass, accreted mass and accreted material composition and initialise them in a star+BH binary (stage 4).

We will perform binary evolutions with Modules for Experiments in Stellar Astrophysics (`MESA`; Paxton et al. 2011) and analyse the final outcomes of the simulations. We assess whether the systems will experience stable mass transfer or common envelope (CE) evolution for systems with different initial conditions. These initial conditions are described by the parameter space spanned by the orbital period ($\log_{10} P_{\rm i}$) and mass ratio ($q_{\rm i} = m_{\rm BH,i}/m_{\rm d,i}$). We adopt the `MESA` framework as described in Marchant et al. (2021), explained in Sect. 2.1. Afterwards, we will

explain the details regarding the accretion process. We will test the behaviour of the accretion models first with a simple exercise where we will investigate the effect on the mass ratio for a fixed period. Later, we will expand on this exercise for a full range of periods to investigate the influence on the entire parameter space, producing detailed grids.

2.1 MESA set up

We perform binary evolution models using version `24.08.1` of the stellar evolution code `MESA`. All input files for the simulations presented in this thesis will be made publicly available on Zenodo[1]. The binary evolution models are produced in a subsolar metallicity environment ($Z = Z_{\odot}/10$) with both relative metal mass fractions and a solar metallicity of $Z_{\odot} = 0.0142$ from Asplund et al. (2009). We consider the following single star physics description in `MESA`. Regarding the equation of state (EOS), `MESA` consider a combination of the EOS from OPAL (Rogers & Nayfonov, 2002), SCVH (Saumon et al., 1995), FreeEOS (Irwin, 2004), HELM (Timmes & Swesty, 2000), PC (Potekhin & Chabrier, 2010) and Skye (Jermyn et al., 2021). The opacity tables and the low temperature opacity tables used in the simulations originate from the OPAL project (Iglesias & Rogers, 1993; Iglesias & Rogers, 1996) and from Ferguson et al. (2005), respectively. The nuclear rates stem from NACRE Angulo et al. (1999), JINA REACLIB Cyburt et al. (2010), and weak reaction rates from Fuller et al. (1985), Oda et al. (1994) and Langanke and Martínez-Pinedo (2000).

Regarding the stellar winds, we incorporate a combination of mass loss rates as described by Brott et al. (2011). For stars with a hydrogen mass fraction $X > 0.7$, we adopt the line-driven mass loss rates from Vink et al. (2001). When this hydrogen mass fraction is lower than 0.4, we take the Wolf-Rayet mass loss rates from Hamann et al. (1995). In the latter case, we account for wind clumping by scaling the mass loss rates with a value of 10 (Yoon et al., 2010). To generate a smooth transition between the two regimes ($0.4 < X < 0.7$), we interpolate between the mass loss rates. When we approach temperatures below the temperature value corresponding with the bistability jump (Vink et al., 2001), we use the following methodology. We consider the mass loss rates from Nieuwenhuijzen and de Jager (1990) and scale this with the factor $(Z/Z_{\odot})^{0.85}$ (see Vink et al. 2001). After scaling, we chose the maximum mass loss rates between the rescaled values from Nieuwenhuijzen and de Jager (1990) and the combination from Vink et al. (2001) and Hamann et al. (1995) as described above.

For the treatment of convection in `MESA`, we use the mixing length theory from Böhm-Vitense (1958). We follow the methodology as described in Cox and Giuli (1968) with a mixing length parameter with the value $\alpha_{\rm MLT} = 2$. We consider the convective regions as dictated by the Ledoux criteria (Ledoux, 1947). A step-overshooting scheme is used for the overshooting of the convective core during the hydrogen burning. The size of the convective core extends with a pressure scale height of $\alpha_{\rm ov} = 0.335$. For this, we follow the calibration described in Brott et al. (2011). However, after the main sequence, a small quantity of exponential overshooting (Herwig, 2000) is incorporated for the subsequent convective regions. This exponential overshooting is described by the length scale of exponential decay of the mixing coefficient of $f = 0.01$. Semiconvective mixing (Langer et al., 1983) is considered with a large efficiency parameter of $\alpha_{\rm sc} = 100$. Aside from semiconvection, we include thermohaline mixing

[1] `https://doi.org/10.5281/zenodo.15630075`

(Kippenhahn et al., 1980) with an efficiency parameter equal to 1.

Regarding the binary physics description in MESA, we include the following. MESA calculates the Roche lobe radii through the numerical fit from Eggleton (1983). For the mass transfer rates, we follow the methodology described in Marchant et al. (2021). The mass transfer rates describing RLOF originate from Ritter (1988). The accretion rate onto the black hole is limited by the Eddington accretion rate as shown in Marchant et al. (2017) (see Sect. 1.2.1). We account for a change in angular momentum as the binary system loses mass by removing the amount of angular momentum related to the specific orbital angular momentum from each component. This mass loss can either be by the donor star losing mass through stellar winds or the ejected material near the BH as the accretion rate exceeds the Eddington limit (see part on isotropic re-emission and the Eddington limit in Sect. 1.2.1). We consider angular momentum loss through GW radiation (Peters, 1964). However, this effect is negligible in comparison to the timescales of the simulated binary evolution. Gravitational radiation will become the single mechanism that will drive the orbital evolution after the formation of the BH+BH binary. We estimate the merger time as described in Peters (1964). We do not include stellar rotation or spin-orbit coupling in the used angular momentum description. We consider not only the situation where the radius of the donor star can exceed its Roche lobe radius but also its outer Lagrangian point and will adapt the angular momentum of the system accordingly following Marchant et al. (2021).

The simulations are terminated once the donor star has reached carbon depletion or when the mass transfer rate exceeds a certain high threshold $\dot{M}_{\rm high}$, indicative of unstable MT and the onset of the CE evolution. In the former case, we assume that the donor star will direct collapse into a BH with the same baryonic mass. If the system has experienced interaction, we flag it as a system that undergoes stable mass transfer. In the latter case, we assume that the system experiences common envelope evolution. The terminating mass transfer rate threshold is chosen to be $\dot{M}_{\rm high} = 1\ M_\odot\ {\rm yr}^{-1}$, well over of the thermal timescale MT rate for the considered systems. We terminate the simulation once the mass transfer rate indicates that the system will experience the CE channel and do not model the outcomes of CE further.

2.2 Hydrogen- and helium-rich accretion models

Without performing the simulation of the first MT phase, there are several methods to mock the accretion process. We decided to study two cases where a considerable amount of mass gets accreted, with a significant difference in accreted mass composition between the two. The objective is to analyse whether the stability is changed in a meaningful way when these extreme conditions are considered.

In this chapter, we consider binary systems composed of a $30\ M_\odot$ mass donor star and a black hole (BH; approximated by a point mass) in a circular orbit in a subsolar metallicity environment ($Z = Z_\odot/10$). The mass $30\ M_\odot$ is chosen as we expect it to be the mass of a BH progenitor, produced via direct collapse. This is chosen to be comparable to the binary evolution models provided in Marchant et al. (2021). To achieve the desired effect of a donor star with a perturbed composition due to prior interaction, we introduce the accretion models. To initiate the process of accretion, we start with a $20\ M_\odot$ mass single star. We let this star evolve until

it has reached a core hydrogen abundance of 0.35. We accrete mass on top of its surface until we reach a star with the desired mass of $30\ M_\odot$ after this core hydrogen abundance is reached, indicating that the onset of this accretion process happens during the main sequence of the donor star (case A). This translates to an accreted mass fraction of 0.5, which is deliberately chosen to heighten the mass transfer effect. This accretion happens on a thermal timescale with a rate of $10^{-3}\ M_\odot\ \mathrm{yr}^{-1}$, which is a faster pace than the evolutionary timescale of the star. For simplicity, we did not consider a two-staged accretion process, but decided to start the accretion process with fast case A on a thermal timescale, without accounting for an additional slow case A MT.

We consider two different accretion models, where we apply the accretion process as described above, but alter the composition of the accreted material. In the first model, we accrete the same surface material (which consists of $X = 0.74765$, $Y = 0.25093$ and the remaining being heavier metals). Since the abundance of hydrogen is higher, we will refer to this as the *hydrogen-rich* accretion model. For the other accretion model, the accreted material is made up of 50% helium ($X = 0.49858$ and $Y = 0.5$) and will be called *helium-rich*. We consider these specific abundance mass fractions to intensify the effect if the majority of the material were to be hydrogen or if the star were to accrete a large amount of helium.

After obtaining these enriched single star models, they are used as the donor star in the donor star with black hole binary starting configuration. We can now investigate the (in)stability when the donor star has a perturbed composition. We will compare the behaviour of the accretion models with a binary configuration where the donor star did not experience this accretion process and is a $30\ M_\odot$ mass ZAMS star (provided by Picco et al., in prep.). This will be referred to as the *non-accretion model*. Before analysing the (in)stability, it is instructive to study the stellar evolution of a single star with the above-described enriched composition and the same mass.

2.2.1 Single star tracks

Fig. 2.1 shows the evolution of a single star that experienced the accretion process as described above, together with a star of the same mass that did not undergo this accretion process. We include the evolution of a $30\ M_\odot$ non-accretion star modelled from ZAMS, to be used as a baseline for comparison. The evolution of the single stars is depicted in the Hertzsprung-Russell diagrams (HRD), where we show luminosity versus decreasing effective temperature of the stars. On these tracks, we mark different nuclear burning stages happening in the core during the single star evolution. Given the radius of the donor star R_d and any mass ratio q_i, we can compute the orbital period P_i that marks the onset of Roche lobe overflow by combining Eq. 1.1 with Kepler's third law. We can translate each nuclear burning stage in the $(\log_{10} P_\mathrm{i}, q_\mathrm{i})$ parameter space with their corresponding radius R_d and component masses (m_d and m_BH):

$$P_\mathrm{i} = \frac{2\pi}{(G(m_\mathrm{d} + m_\mathrm{BH}))^{3/2}} \left(\frac{R_\mathrm{RL}}{a}\right)\Big|_{q_\mathrm{i}}^{3/2} R_\mathrm{d}^{3/2}. \tag{2.1}$$

By comparing the outcomes of the accretion models to those where the donor is initialised as a ZAMS star, we see several interesting results. In the case where the accreted material is hydrogen-rich, we see that the evolutionary track before the MT is very similar to that of

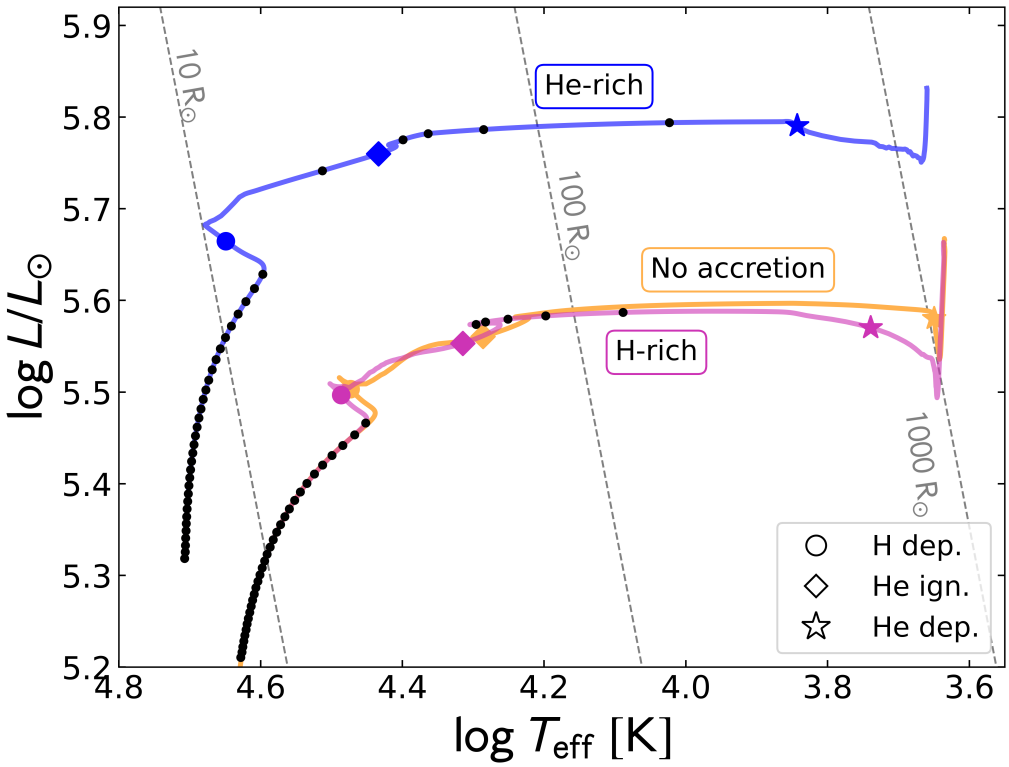

Figure 2.1: Hertzsprung-Russell diagrams of both accretion models compared to a $30\ M_\odot$ mass star initialised at ZAMS that did not undergo the accretion process indicated in yellow. Hydrogen-rich accretion model is shown in pink and helium-rich model in blue. Different markers correspond to different stages reported in the legend. Dashed lines in the background mark different stellar radii. Dots represent constant intervals of 10^5 years in stellar age.

a ZAMS star of the same mass, with only a slight increase in effective temperature during the majority of the evolution. This indicates that the hydrogen-enriched single star quickly adjusts to its new mass. However, at late evolutionary stages, we see that the hydrogen-rich star diverges from that of the unperturbed $30\ M_\odot$ evolution, appearing to be less luminous. By looking at the black dots on top of the evolutionary track of the hydrogen-enriched star, we see that this star evolves more slowly after core helium ignition. If we consider the helium-enriched accretion model, the evolutionary tracks differ more significantly. At every evolutionary phase, the helium-enriched star is hotter than the unperturbed $30\ M_\odot$ mass star. The tracks also show that the helium-rich star has an increased luminosity throughout its evolution and is more compact. In Chapter 3, we will see that this can affect the occurrence of case A mass transfer after the formation of the BH (stage 6a).

2.3 Stability boundary at fixed period

Before investigating the (in)stability of an extended parameter space spanned by the orbital period and mass ratio of the binary systems, we will explain the method used to evaluate the stability. The *stability boundary* is defined by the critical mass ratio value $q_{\rm crit}$ threshold below which mass transfer is unstable. For all systems with a mass ratio higher than this critical value $q_{\rm crit}$, the binary experiences stable mass transfer. In order to find the stability boundary,

we use a bisection search algorithm, which we will illustrate for a fixed period of $P_{\rm i} = 100$ days. We select this value arbitrarily at a period where we know the system will interact.

We start the bisection search with the lower and upper initial mass ratio values of near zero and unity, respectively. We assume that the lower mass ratio value ($q_{\rm i,low}$) experiences unstable common envelope evolution and the upper mass ratio value ($q_{\rm i,upp}$) undergoes stable mass transfer. To start the search, we investigate the (in)stability of the average of $q_{\rm i,low}$ and $q_{\rm i,upp}$, resulting in a mass ratio value of $q_{\rm i,mid}$. If the simulation at this value undergoes stable mass transfer, we update to higher mass ratios $q_{\rm i,upp}$ by $q_{\rm i,mid}$ and the next simulation will start with their new average value. In the case where the binary evolution would result in common envelope evolution, we work analogously but now update $q_{\rm i,low}$ by $q_{\rm i,mid}$. We apply this algorithm on all three discussed models (non-accretion, hydrogen-rich and helium-rich) for a fixed period of $P_{\rm i} = 100$ days and repeat this process for eight iterations. We used the limit of $q_{\rm i,low} = 0$ and $q_{\rm i,low} = 1$.

The bisection algorithm divides the interval in two for each iteration and thus, after n iterations, the distance between each evaluation scales with $\sim 1/2^n$. If we were to use n uniformly spaced points in the mass ratio interval, the distance between each point would be the same size and scale as $\Delta q \sim 1/n$. We would have to use many more samples to achieve the same precision that we can reach with the bisection search. Using the bisection algorithm for finding the stability boundary therefore reduces the computational cost. To investigate the (in)stability,

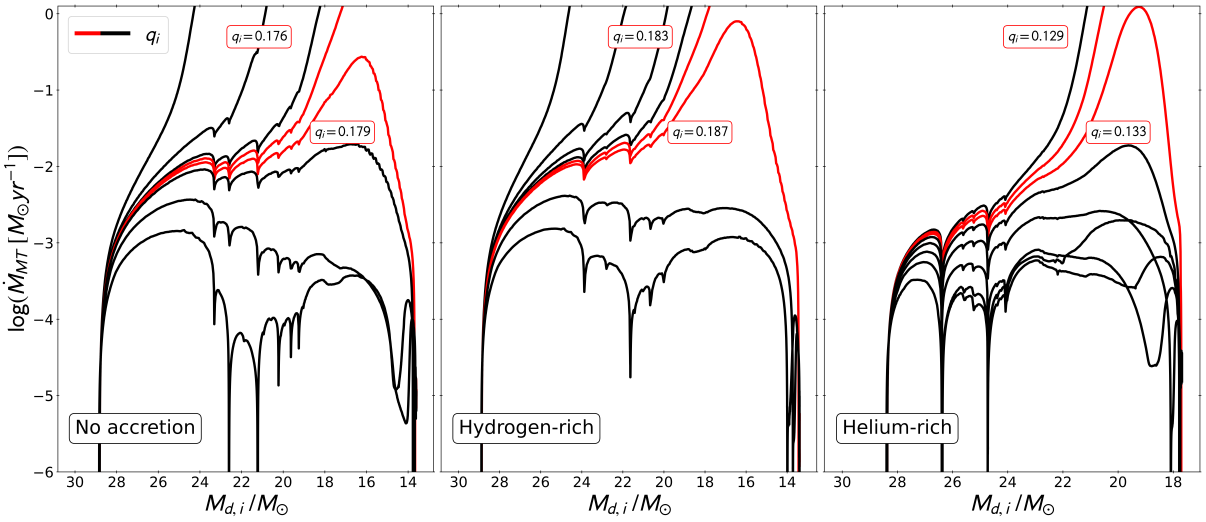

Figure 2.2: The mass transfer rates versus decreasing donor mass for all eight iterations of the bisection at a fixed period of $P_{\rm i} = 100$ days. Red indicates the last two iterations of the bisection search, marking the edges of the range where the critical mass ratio exists. *Left:* Non-accretion model. *Middle:* Hydrogen-rich accretion model. *Right:* Helium-rich accretion model.

we can evaluate the behaviour of the mass transfer rate $\dot{M}_{\rm MT}$. This is done by looking at curves displaying the mass transfer rate versus the mass of the donor star as the donor loses mass to the accretor during the mass transfer. When the donor star fills its Roche lobe, the interaction begins and the mass transfer rate starts to increase. Since the unstable common envelope evolution results in ever-increasing mass transfer rates, this will reflect in those curves

too. On the one hand, for the systems that undergo common envelope evolution, these curves will keep increasing with the MT, until they reach the maximum threshold. On the other hand, in the case of stable mass transfer, these curves will reach a peak and will decrease again as the donor star contracts in response to its mass loss.

The results of the bisection search at a fixed period for the non-accreted model and both accretion models are shown in Fig. 2.2. For the non-accretion model, we find after eight iterations that the critical mass ratio exists in the range $q_{\rm crit} \in [0.176; 0.179]$ for the fixed period. We perform the same bisection search for eight iterations for both accretion models. In the hydrogen-rich case, the critical mass ratio exists in the $q_{\rm crit} \in [0.183; 0.187]$ range. On the other hand, the helium-rich models appear to have a critical mass ratio within the $q_{\rm crit} \in [0.129; 0.133]$ range. Note that these regions can be further reduced by adding more iterations. Compared to the non-accretion model, we see only a small shift in the critical mass ratio range of the hydrogen-rich accretion model to higher values. In contrast to this, we see a significant shift to lower mass ratio values for the helium-rich accretion models. This shows that for this period ($P_{\rm i} = 100$ days), the stability boundary shifts for both accretion models, therefore hinting towards the influence of a perturbed stellar interior on the full parameter space.

2.4 Detailed grids

By performing the above-described bisection search for the critical mass ratio $q_{\rm crit}$ for a full range of periods, we can produce the stability boundary in the $(\log_{10} P_{\rm i}, q_{\rm i})$ parameter space (period is expressed in days). In an analogous method, one can also search for the boundary of systems that undergo stable MT where $t_{\rm merge} = 13.8$ Gyr (the age of the Universe). This boundary separates the binaries that are too wide to merge within the age of the Universe and those that are close orbit binaries that are tight enough to have a merger time below 13.8 Gyr. By connecting the stability boundary and the $t_{\rm merge} = 13.8$ Gyr boundary, we can build regions in the $(\log_{10} P_{\rm i}, q_{\rm i})$ parameter space. These regions represent the predicted systems that can produce a gravitational wave signal through a BH merger that experienced stable mass transfer.

We provide grids of binary evolution for the three models (non-accretion, hydrogen-rich and helium-rich) with a $30\ M_\odot$ mass donor star with a BH companion in a circular orbit. The masses of the BH accretor are variable since they are computed by the range of initial mass ratios $q_{\rm i} = m_{\rm BH}/m_{\rm d,i}$. We consider the outer edges of the mass ratios range to be between $q_{\rm i} = 0.005$ and $q_{\rm i} = 1$. For each value of the range in periods, we perform the bisection algorithm for 10 iterations.

It has been shown that the stability boundary significantly shifts to higher mass ratio values at higher periods when the envelope starts becoming convective (Hjellming & Webbink, 1987). To evaluate this behaviour, we select a finer (fixed) resolution at the period where the envelope of the star starts to become convective. The additional resolution in the period is used for the widest systems that interact after the development of a convective envelope. The ranges and resolution for the three models of both grid panels above this value ($\log_{10} P_{\rm i,high}$) and below ($\log_{10} P_{\rm i}$) this value is shown in Table 2.1.

The resolution of the lower panel of periods is defined to be the resolution that corresponds to 30 different period values. The higher resolution of the upper panel corresponds to an equal amount of 30 period values with at least 1 period value (the highest) that serves as an upper limit where no interaction happens. Therefore, each grid will calculate the critical mass ratio for the (in)stability and where $t_{\rm merge} = 13.8$ Gyr for 61 period values in total. The simulation

Table 2.1: The ranges and resolution of two panels of the grid that are separated by the period value, where the donor star experiences a convective envelope (1 % of the total mass of the star). Period is expressed in days.

Model	No accretion	Hydrogen-rich accretion	Helium-rich accretion
start $\log_{10} P_{\rm i}$	-0.444	-0.273	-0.455
end $\log_{10} P_{\rm i}$	2.946	2.937	2.935
$\Delta \log_{10} P_{\rm i}$	0.133	0.107	0.113
start $\log_{10} P_{\rm i,high}$	2.946	2.937	2.935
end $\log_{10} P_{\rm i,high}$	3.456	3.447	3.505
$\Delta \log_{10} P_{\rm i,high}$	0.017	0.017	0.019

of each grid will have several terminating conditions to assess the outcomes of the considered binary systems. We span a parameter space starting from low periods where the binary can experience Roche lobe overflow at the zero-age main sequence of the donor star, up to high periods where the components are in an orbit too wide to undergo interaction. We evaluate the outcomes of the binary evolution that either experiences common envelope evolution or stable mass transfer.

2.4.1 Results

In Fig. 2.3, we show a summary of all final outcomes of simulations of both accretion models. The same plot for the non-accretion model grid can be found in the Appendix (A1). We indicate evolutionary stages as grey lines on the background of these grids of simulations corresponding with the stages marked in the single star tracks from Fig. 2.1. These represent what evolutionary phase the donor is at the onset of mass transfer to indicate if the system undergoes case A, B or C mass transfer and are calculated by Eq. 2.1 as described in Sect. 2.2.1.

At higher periods (upper panel), we see that, as expected, the stability boundary makes a bend towards higher mass ratios, creating a hook in the boundary that separates the systems experiencing CE and those that undergo stable MT. For the helium-rich model, this bend allows for a smaller area of systems that experience the CE evolution compared to the hydrogen-rich model. Regarding the systems that survive the CE phase producing tight orbit BH binaries and the relation with the envelope being convective in order for this to happen, we refer to Marchant et al. (2021). The systems experiencing stable MT in a close enough orbit for the binary BH to merge within the age of the Universe are indicated in yellow in Fig. 2.3. On first glance, we can see that the helium-rich accretion models predict a large area in the parameter space that allows for these close binaries to be produced by stable MT. To investigate the behaviour of these systems in more detail, we can outline their area in the parameter space by connecting their stability boundary and boundary where $t_{\rm merge} = 13.8$ Gyr. This results in the regions being shown in Fig. 2.4.

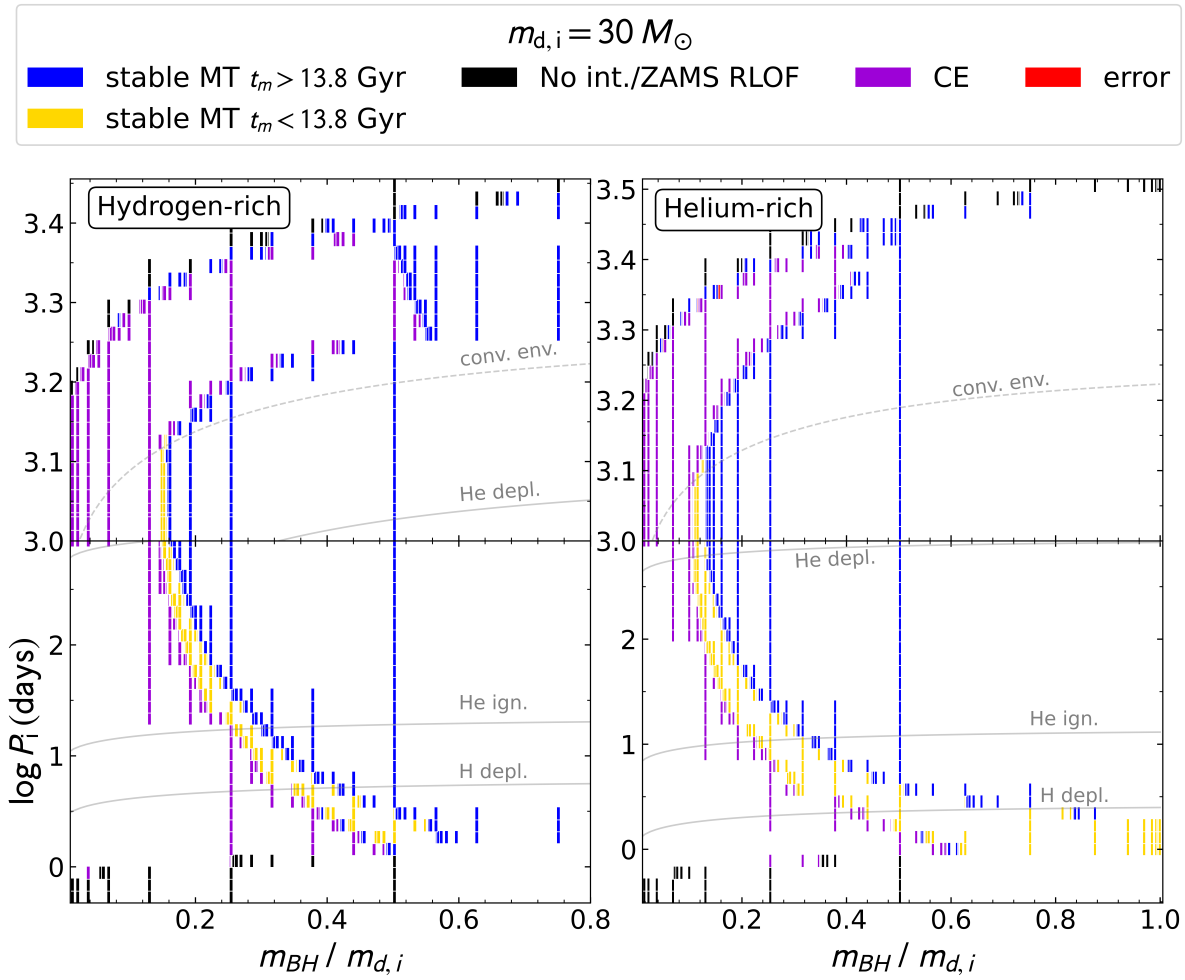

Figure 2.3: Summary of final outcomes of the simulations using the bisection algorithm to find predicted BH mergers that experienced stable MT (yellow). Horizontal lines indicate different evolutionary stages of a single star with the same initial mass as the donor star. Solid lines mark hydrogen depletion and helium ignition. Dashed line in the upper panels shows where the star starts to have a 10% convective envelope.

With the regions in Fig. 2.4 we can compare both accretion models and the non-accretion model to one another. For the hydrogen-rich accretion model, we see that there is a small shift compared to the non-accretion model for high periods, but overall, there is no significant change. In contrast to this, if we consider the helium-enriched accretion model, the area of predicted BH mergers of the stable MT region differs. In this case, the conditions for BH mergers after an orbital shrinkage through stable MT shift significantly, accessing systems with more extreme mass ratios for high periods. For shorter periods, we see a significant range of mass ratios being allowed for stable MT. In general, we can see that the separation between the stability boundary and the boundary where $t_{\rm merge} = 13.8\ {\rm Gyr}$ is larger for the helium-rich accretion model compared to the other two. At a period of $\log_{10} P_{\rm i} \approx 1.5\ (30\ {\rm days})$, the region of helium-rich accretion model starts to deviate from the other two regions and its $t_{\rm merge} = 13.8\ {\rm Gyr}$ boundary can reach even lower mass ratios than the stability boundary of the hydrogen-rich and non-accretion model. We do not know the population distribution for

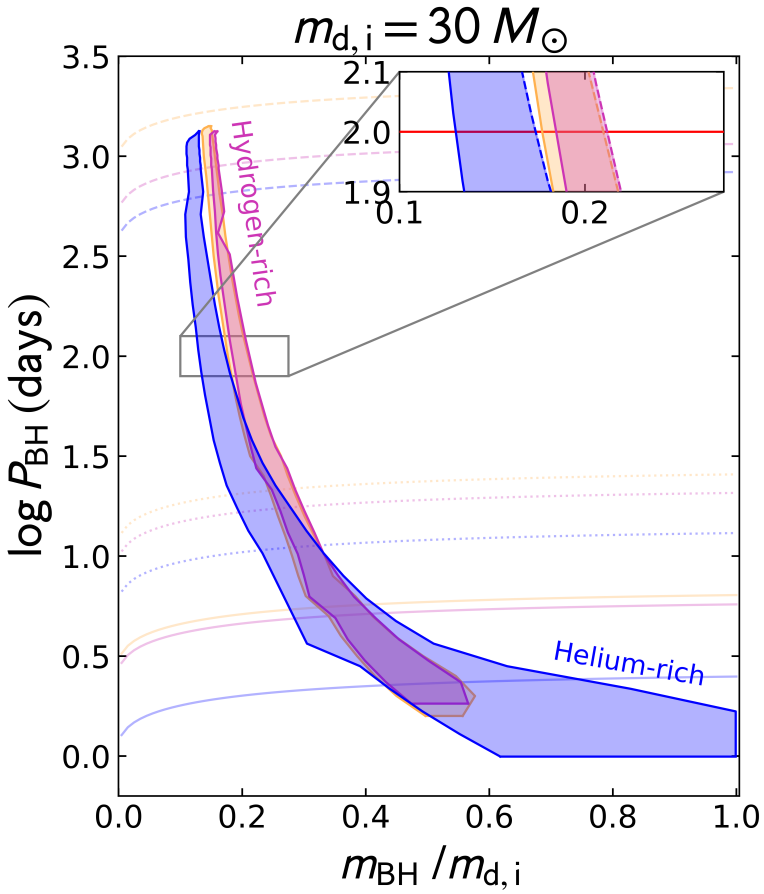

Figure 2.4: Regions describing systems that undergo the stable MT channel that leads to merging binary BHs within the age of the Universe for the non-accretion model (gold), the hydrogen-rich accretion model (pink) and the helium-rich accretion model (blue). Lines on the background indicate different evolutionary tracks. Solid lines represent core hydrogen depletion, dotted lines mark the ignition of central helium and the dashed upper lines are where core helium is depleted. Close-up of the behaviour of the critical boundaries near $P_{\mathrm{i}} = 100$ days (red line).

the mass ratios and periods of star+BH systems in nature. If we assume a flat distribution for both parameters, the relative contribution of all three models can be determined by their relative areas in Fig. 2.4. By doing so, we get a ratio between the non-accretion model and the hydrogen-rich accretion model of 1.196 systems inside the region. By comparing the non-accretion model to the helium-rich accretion model, we find a fraction of 0.372. This indicates that accounting for a previous MT (stage 2) leads to almost a 3-fold increase in the production of merging BH+BH systems.

We can calculate ranges of the final mass ratios of the predicted binary BH mergers through the stable MT channel. This final mass ratio ($q_{\mathrm{f}} < 1$) represent the mass ratio of the system when the second BH is formed, i.e., the BH+BH stage (stage 7a) and is the one that is detectable through gravitational wave signals (see Eq. 1.13). Note that to be consistent with the notation of the Gravitational Wave Transient Catalogue ($q_{\mathrm{f}} < 1$), we provide the minimum value as $m_{\mathrm{f,min}} = \min\{\mathrm{m_{f,BH}/m_{f,d}; m_{f,d}/m_{f,BH}}\}$. In the latter case, the mass ratio is inverted

providing a BH with a mass more massive after the mass transfer stage (stage 6a). For the non-accretion model, we see that the minimum value of the final mass ratio is $q_{\rm f,min} = 0.296$. For the hydrogen-rich accretion model we find values of $q_{\rm f,min} = 0.332$, while for the helium-rich accretion models we calculate $q_{\rm f,min} = 0.183$. Due to the final resolution of the computed grids, we will not reach mass ratios of exactly unity, however since we calculate maximum values of $m_{\rm f,BH}/m_{\rm f,d}$ higher then unity for all three models, we can include unity and mark this as the upper limit of final mass ratios. We see the same trend occurring in these ranges of final mass ratios, namely a slightly smaller range for the hydrogen-rich model compared to the non-accretion model, but a significant increase in range for the helium-rich model.

Chapter 3

End-to-end Binary evolution models

To properly report on the physics behind the mass transfer phase before the formation of the first black hole (BH; stage 2 in Fig. 1.6) and its effect on the formation channels to produce binary BH mergers, one has to consider models initialised with two zero-age main sequence stars (ZAMS). Therefore, in this chapter, we explore an *end-to-end* models of a set of massive binaries with the stellar evolution code `MESA`. By doing so, we include the history happening before the formation of the first black hole. In Chapter 2, we assumed a flat distribution of the periods and mass ratios of all probed systems at the star+BH stage. By initialising both stars at ZAMS, we directly probe the mass ratios and periods of the star+BH stage (stage 4) as they are predetermined by the initial conditions at the ZAMS+ZAMS stage, which is well informed observationally. In addition to this, we do not have to rely on arbitrary choices for the properties and accretion process.

The accretion models of Chapter 2 are, by design, a flexible method to manipulate the past accretion process that the donor star encountered. The method of the end-to-end evolution of this chapter does not offer us the same amount of control. Since we are modelling a full binary evolution, this raises the complication of matching up the masses with the desired $30\ M_\odot$ donor mass considered in Chapter 2. Therefore, we cannot produce a direct one-to-one comparison of the results of the end-to-end simulation with those of the accretion models or results presented in literature. However, it is still instructive to do a comparison between the two developed methods. We will calculate the accretion mass fraction (accreted mass by total mass) and composition of this accreted mass to compare this with the ones assumed in Chapter 2.

The grid of simulations will be considered in a $(\log_{10} P_\mathrm{i}, q_\mathrm{i})$ parameter space similar to Chapter 2. To avoid confusion, we will refer to the component masses of the binary as the primary and the secondary (primary being the initially most massive one) instead of the donor and accretor, since we are considering two different mass transfer stages where their respective roles invert. We will define the mass ratio vs period parameter space right after the formation of the first BH (stage 4) as $(\log_{10} P_\mathrm{BH}, q_\mathrm{BH})$ where $q_\mathrm{BH} = m_\mathrm{BH}/m_2$. As such, we can compare these properties to the parameter space probed in Chapter 2.

In this chapter, we will provide a brief section on the methodology used to perform the grid of end-to-end simulations. Afterwards, we show the end results of the grid for each initial configuration. We will finalise this chapter with a comparison between the results and properties of the end-to-end simulation and the accretion models to investigate the robustness of this

latter method.

3.1 Methods

We adopt most of the MESA methodology as described in Chapter 2, with some minor adjustments to account for processes that appear when modelling a full binary evolution. The full binary evolution simulations start with two massive stars at ZAMS (stage 1). Assuming that the most massive star will evolve faster, this star will exceed its Roche lobe radius first and transfer mass onto its companion. In these simulations, we consider the first mass transfer episode from the primary star to the secondary star to be fully conservative (with the exception of wind mass loss). Once the more massive star reaches carbon depletion, we assume that the star will experience core collapse and form a BH with the same mass as its baryonic mass. We automatically turn this star into a point mass to treat the formation of a BH with MESA. After the first BH is formed, we perform simulations with the same set-up as described in Chapter 2 to model the remaining evolution.

We compute a grid of models starting with a fixed donor star of $m_{1,\mathrm{i}} = 40\ M_\odot$ in a circular orbit around an accretor star with variable masses denoted as $m_{2,\mathrm{i}}$. The primary mass was chosen high enough that it would still be considered inside the BH progenitor mass regime, knowing that it would lose mass to its companion. The environmental subsolar metallicity is the same as for the accretion models of $Z = Z_\odot/10$, as well as the value of $\alpha_{\mathrm{ov}} = 0.335$. We consider a parameter space of initial configurations with the variables being the initial mass ratio ($q_{\mathrm{i}} = m_{2,\mathrm{i}}/m_{1,\mathrm{i}}$) and initial orbital period ($\log_{10} P_{\mathrm{i}}$). The grid spans over mass ratios from $q_{\mathrm{i}} = 0.2$ to $q_{\mathrm{i}} = 1$ with a resolution of $\Delta q_{\mathrm{i}} = 0.05$. This translates to a lowest accretor mass of $m_{2,\mathrm{i}} = 8\ M_\odot$, which is still considered a massive star. We do not probe mass ratios lower than $q_{\mathrm{i}} = 0.2$ to avoid the unstable common envelope evolution producing stellar mergers. The initial period values range between $-0.3 < \log_{10}(P_{\mathrm{i}}/\mathrm{d}) < 3$ with a resolution of $\Delta \log_{10}(P_{\mathrm{i}}/\mathrm{d}) = 0.2$. This range will include the systems that can experience Roche lobe overflow at ZAMS. Note that the goal of this thesis is to probe systems generating GW signals through stable mass transfer; we do not need to investigate a finer resolution panel for higher periods, as described in Chapter 2. In total, we perform a grid of 272 full end-to-end binary simulations.

3.1.1 Endpoints of simulations

We are probing the systems that evolve into binary BH mergers, producing GWs through stable mass transfer from the star to the BH. However, there are other possible evolutionary end-points that we need to account for. The binaries can experience Roche lobe overflow during their zero-age main sequence at small periods (ZAMS RLOF).

Another possible outcome that does not appear in Chapter 2 is what we call *Accretor Overflow*. Before the formation of the BH, the accretor star starts can overflow its Roche Lobe during or after the first MT phase (stage 2), both potentially triggering the unstable common envelope phase. Therefore, we terminate the system if this occurs. Additionally, we take care of systems that might end up with inverse mass transfer for the simulations with a mass ratio close to unity. To account for this, we terminate the binary simulations where the secondary star

reaches hydrogen depletion while the primary is still evolving on the main sequence. This would indicate that the secondary star would start exceeding its Roche lobe radius before the primary and thus transfer mass from secondary to primary instead of the other way around, as desired. These systems will be flagged as systems experiencing an *Inverse Mass Transfer* (Inverse MT).

All systems that survive the above-mentioned terminating conditions reach the star+BH stage. Since all of these systems are stable, we only separate the systems experiencing stable MT (second MT phase; 6a) between the ones with a merger time above $13.8\ \mathrm{Gyr}$ and those below. We adopt the same conditions for stable MT as described in Chapter 2. Once the secondary star reaches carbon depletion, we assume core collapse and terminate the simulation, while marking the system as one that undergoes stable MT. However, some systems do not show any interaction after the first BH is formed (No int.).

3.2 Results

Before investigating the final fates of the end-to-end simulations, we will first take a closer look at the stellar evolution track of a single star with the same mass as the primary star ($m_{1,\mathrm{i}} = 40\ M_\odot$). Fig. 3.1 shows the Hertzsprung-Russell diagram (HRD) of a $40\ M_\odot$ star in the physical conditions as described in Section 3.1.

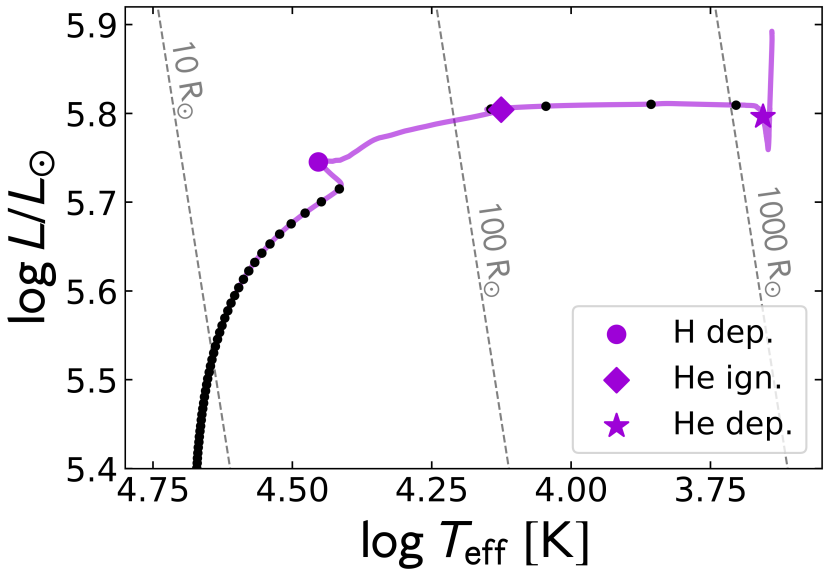

Figure 3.1: HRD of a $40\ M_\odot$ single star with subsolar metallicity. Different evolutionary stages are indicated by the markers (hydrogen depletion, helium ignition and helium depletion). The black, smaller dots represent constant intervals of 10^5 years in stellar age. Lines in the background indicate different stellar radii.

The final endpoints of the end-to-end binary evolution models with a $m_{1,\mathrm{i}} = 40\ M_\odot$ initial primary star and a subsolar metallicity $Z_\odot/10$ is shown in Fig. 3.2. This figure shows different evolutionary stages of a $40\ M_\odot$ single star in white to indicate different boundaries for interaction, which are calculated with Eq. 2.1 from the single star evolution shown in Fig. 3.1.

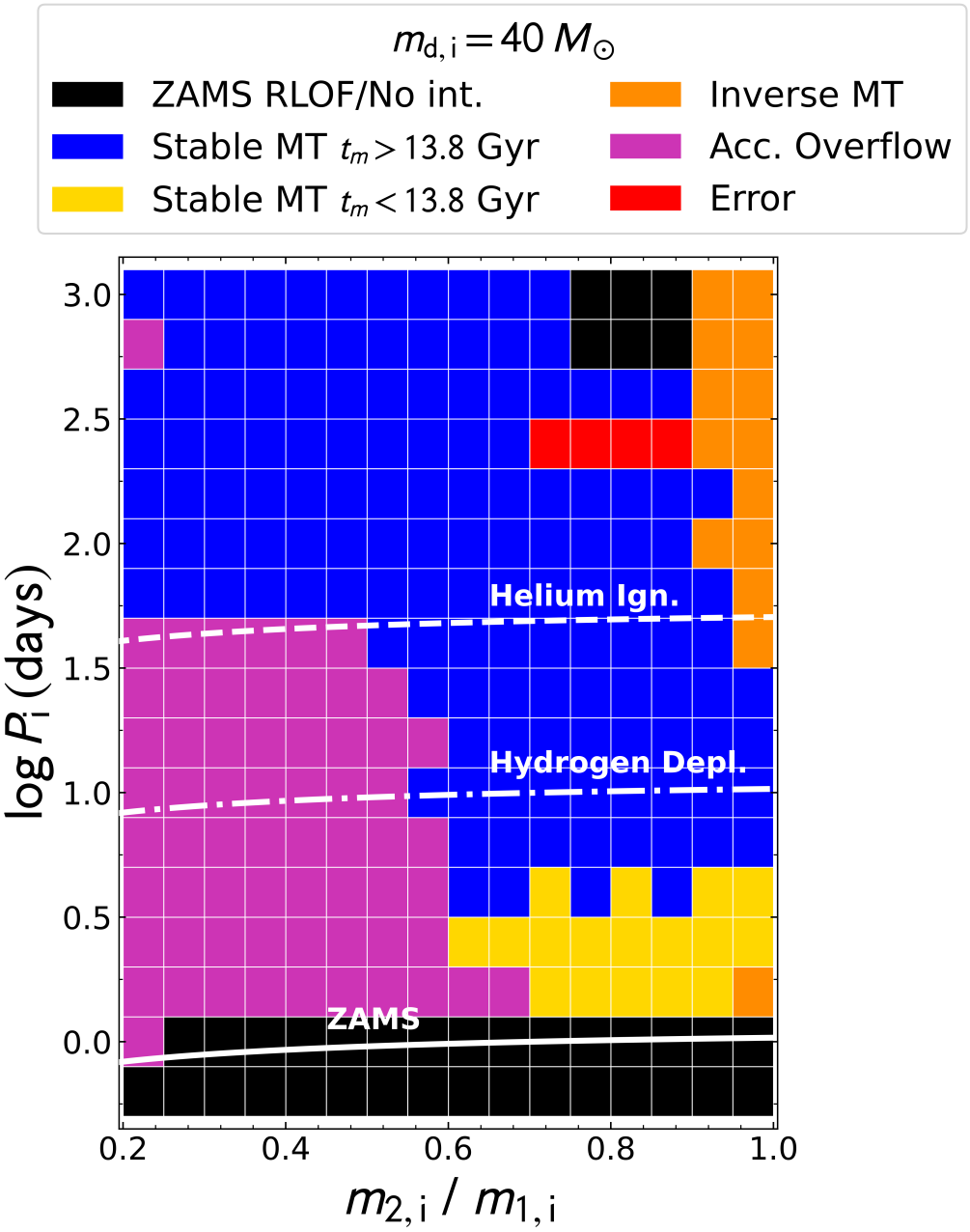

Figure 3.2: Summary of the final fates of end-to-end simulations starting out with a fixed primary star mass of $40\ M_\odot$ in a circular orbit with its companion. Black indicates either ZAMS RLOF or no interaction after the formation of the first BH. We separate systems experiencing stable MT after formation first BH by $t_{\rm merger} > 13.8$ Gyr (blue) and $t_{\rm merger} < 13.8$ Gyr (yellow). We mark inverse MT with orange and accretor overflow with pink. Simulations that did not converge are indicated in red. The white lines indicate different evolutionary stages of the primary star taking place during the first interaction. The dash-dotted line marks hydrogen depletion and the dashed line marks helium ignition.

Fig. 3.2 shows that the lower part of the $(\log_{10} P_{\rm i}, q_{\rm i})$ parameter space is mainly populated by systems experiencing RLOF already at ZAMS when $\log_{10} P_{\rm i} < 0$ (black). This is confirmed by the fact that all of these systems align with or exist below the solid line indicating

ZAMS. At high periods $\log_{10} P_{\rm i} \geq 2.8$, we see six simulations that indicate that there was no interaction between the secondary star and the BH after the BH was formed. Note that these systems did interact before the formation of the BH and thus the secondary star of these systems did undergo accretion. We see that, towards the high initial mass ratios above $q_{\rm i} \geq 0.925$, there are multiple systems that are flagged with *Inverse Mass Transfer* (orange). For these systems, the companion star reaches the end of the main sequence before the primary finishes core-helium burning, leading to inverse mass transfer. The systems located at initial mass ratios of approximately $q_{\rm i} < 0.6$ and $\log_{10} P_{\rm i} < 1.6$ terminate due to the accretor overflowing its Roche lobe during MT, leading up to a contact system (pink). This region cuts off at the $\log_{10} P_{\rm i}$ value that corresponds with the helium ignition line. The majority of the modelled systems, however, are systems that experience stable MT after the primary star turns into a BH. From this majority, there are 136 systems that end up in a binary orbit that is too wide to merge within the age of the Universe and 17 systems with a calculated merger time below 13.8 Gyr (yellow). Therefore, more than half of the simulations in the grid experience stable MT (the exact fraction being 0.566), from which a 0.063 fraction are predicted to result in a binary BH merger. These systems favour the low period and high mass ratio parameter space between $0.2 < \log_{10} P_{\rm i} < 0.6$ and $0.6 < q_{\rm i} < 1$, below the core hydrogen depletion curve. This means that these predicted BH mergers experience case A mass transfer before the first BH is formed.

In Fig. 3.3 we show the periods and mass ratios at the evolutionary point where the first BH is formed. It is also instructive to study how the binaries that evolve into binary BH mergers through stable MT behave at the stage when the first BH is formed, since this is the stage where we start our simulations of Chapter 2. Therefore we provide Fig. 3.3 that shows the position in the $(\log_{10} P_{\rm BH}, q_{\rm BH})$ plane. Here $P_{\rm BH}$ represents the period of the system at the star+BH stage and $q_{\rm BH}$ is defined as $q_{\rm BH} \equiv m_{\rm BH}/m_2$. The colours in this figure are the same as the colours of the final outcomes from Fig. 3.2. In this figure, the scatter points representing wide binaries that experienced stable MT exist in binaries with mass ratios $q_{\rm BH} \gtrsim 0.4$ and periods above $\log_{10} P_{\rm BH} \gtrsim 0.7$ directly after the formation of the first BH. We see that the systems forming BH mergers through stable MT within the age of the Universe populate periods of $0.5 < \log_{10} P_{\rm BH} < 1$ and mass ratios of $0.3 < q_{\rm BH} < 0.45$ approximately. Additionally, we see that the scatter points follow titled lines. This trend occurs due to the relation shown in Eq. 1.10, which maps the initial orbital periods and mass ratios to specific final conditions in a non-linear way.

In Fig. 3.3, we have indicated with different markers if the mass transfer before (stage 2) and after (stage 4) the formation of the first BH appears to be case A, B or C mass transfer. This is calculated by identifying when the second interaction stage occurs and evaluating whether this happens before hydrogen depletion (case A), between hydrogen and helium depletion (case B) or after helium depletion (case C). In the left panel, we see that the systems at lower periods undergo case A MT before the formation of the first BH, but the wide orbit binaries experience case B MT. The right panel shows that most systems experiencing the stable MT formation channel interact as case B mass transfer after the formation of the first BH, with a few systems that encountered case C mass transfer at higher periods. However, if we only consider the predicted BH mergers (yellow), there is one single system marked by case A mass transfer. Do note that this one simulation started mass transfer near the boundary that marks hydrogen depletion, thus late in its main sequence.

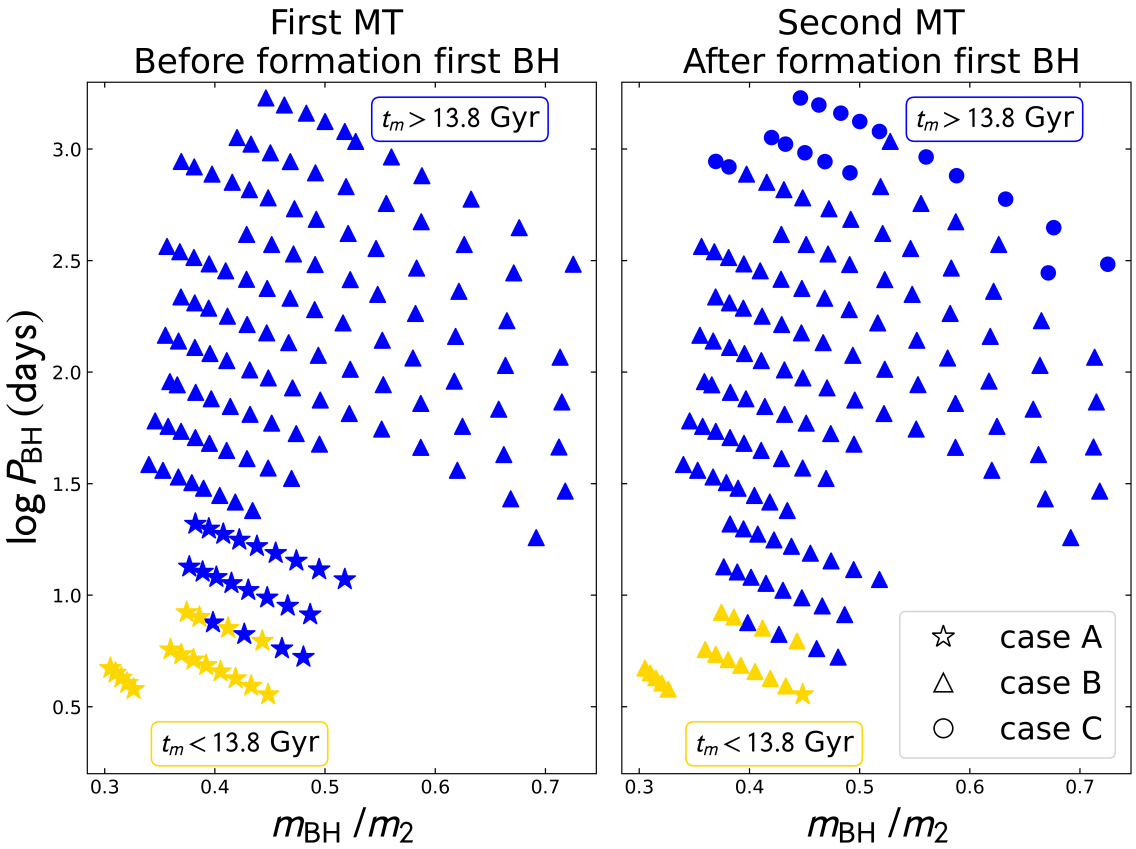

Figure 3.3: The parameter space of all systems experiencing stable MT at the evolutionary stage when the first black hole is formed. Different markers indicate different evolutionary stages of the donor star at the onset of mass transfer, happening before and after the formation of the first BH: case A (stars), case B (triangle up) and case C (circle). Colours represent wide binaries with $t_{\rm merger} > 13.8$ Gyr (blue) and the predicted BH mergers with $t_{\rm merger} < 13.8$ Gyr (yellow).

We can investigate the behaviour of the period and mass ratio ($m_{\rm BH}/m_2$) at the point where the first black hole is formed compared to their initial orbital period ($\log_{10} P_{\rm i}$) and the initial mass ratio ($m_{2,\rm i}/m_{1,\rm i}$). This is shown in Fig. 3.4. The left panel in this figure shows that as $m_{\rm BH}/m_2$ decreases, the initial mass ratio increases. This states that when the initial mass ratio is close to unity, the value of $m_{\rm BH}/m_2$ becomes more extreme and vice versa. The right panel shows that $\log_{10} P_{\rm i}/P_{\rm BH}$ increases as $\log_{10} P_{\rm BH}$ increases. Since the periods are higher compared to their initial values, we see that the interaction before the formation of the BH (stage 2) mainly widens the orbit of the systems, as expected. However, at high mass ratios we see that there are a few systems whose orbit shrinks. Do note the change between the initial period and the period at star+BH stage varies with an approximate absolute maximum value of $\log_{10} P_{\rm i}/P_{\rm BH} \approx 0.5$, which leads to an increase with a factor of 3. Additionally, we calculate the final mass ratios of the resulting BH+BH binary (at stage 7a). We find that for the modelled systems that experience the stable MT channel with merger times within the age of the Universe provide a minimum final mass ratio of $q_{\rm f,min} = 0.418$ and a maximum final mass ratio of $q_{\rm f,max} = 0.706$ (below unity). Compared to the final mass ratio values calculated

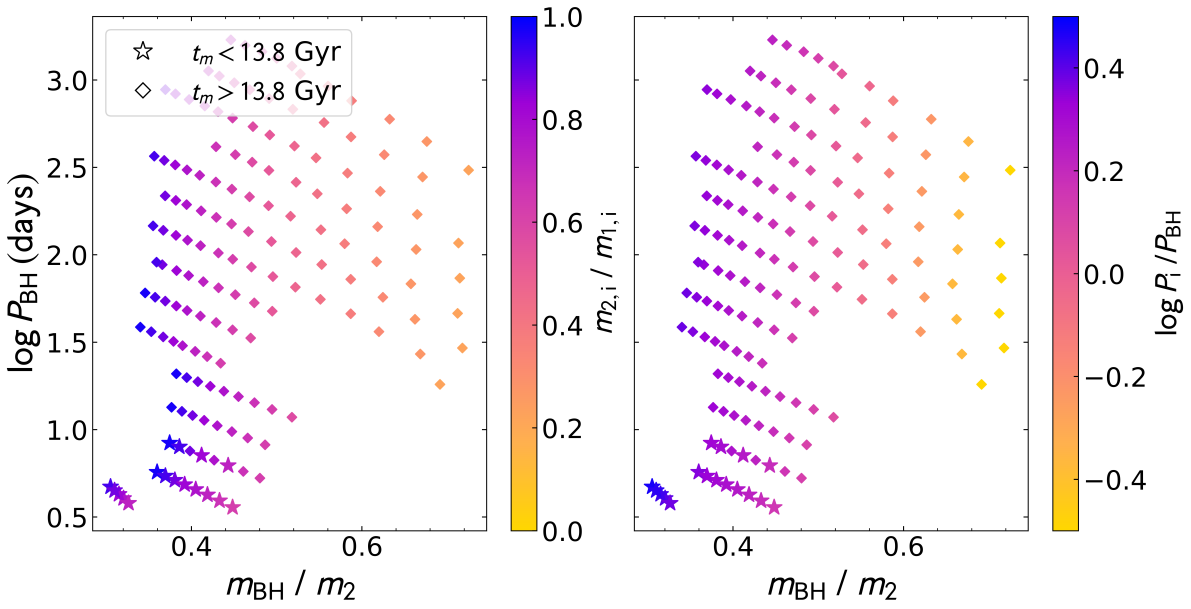

Figure 3.4: Identical parameter space as displayed in Fig. 3.3 but with an additional third dimension. Stars indicate systems experiencing stable MT with $t_{\rm merger} < 13.8$ Gyr and with diamonds if $t_{\rm merger} > 13.8$ Gyr. *Left:* Colour bar indicates the fraction of initial period and period at star+BH stage. *Right:* Colour bar indicated the initial mass ratio.

in the previous chapter, we can see that, again, the end-to-end simulations provide a limited range. Most importantly, we see that the end-to-end simulation can give us a restriction on the maximum final mass ratio as well instead of only a minimum value, excluding unity.

3.3 Comparison to accretion models

In Chapter 2, we introduced an artificial accretion process where we accreted $10\ M_\odot$ on top of a $20\ M_\odot$ star to get the desired $30\ M_\odot$ star, which translates to an accreted mass fraction of 0.5. We analysed two different composition scenarios. The first (hydrogen-rich) accretion model had a hydrogen mass fraction of $X = 0.74765$ and a helium mass fraction of $Y = 0.25093$. The second (helium-rich) accretion model contains a hydrogen mass fraction of $X = 0.49859$ and a helium mass fraction of $Y = 0.5$. Here we will question these assumptions and compare them to the values provided by the full end-to-end simulations. Before doing so, we need to take note that the accretion models start out with a fixed donor mass of $30\ M_\odot$. This would correspond with the mass of the secondary star of the end-to-end simulation when the primary turns into a BH. However, the masses of the secondary star at the point where the first BH is formed are between $43.4\ M_\odot$ to $56.2\ M_\odot$ (for the systems experiencing stable MT with $t_{\rm merger} < 13.8$ Gyr). Therefore, this does not offer a direct one-to-one comparison, but it is still informative to look at the behaviour of the accretion processes before the first BH formation. A scatter plot of all systems experiencing stable MT displaying the masses of their secondary star at the point of the formation of the first BH can be found in the Appendix (Fig. A2).

We will perform the comparison between the scatter plot shown in Fig. 3.3 and the results from the accretion models shown in Fig. 2.4. This is presented in Fig. 3.5. We see that

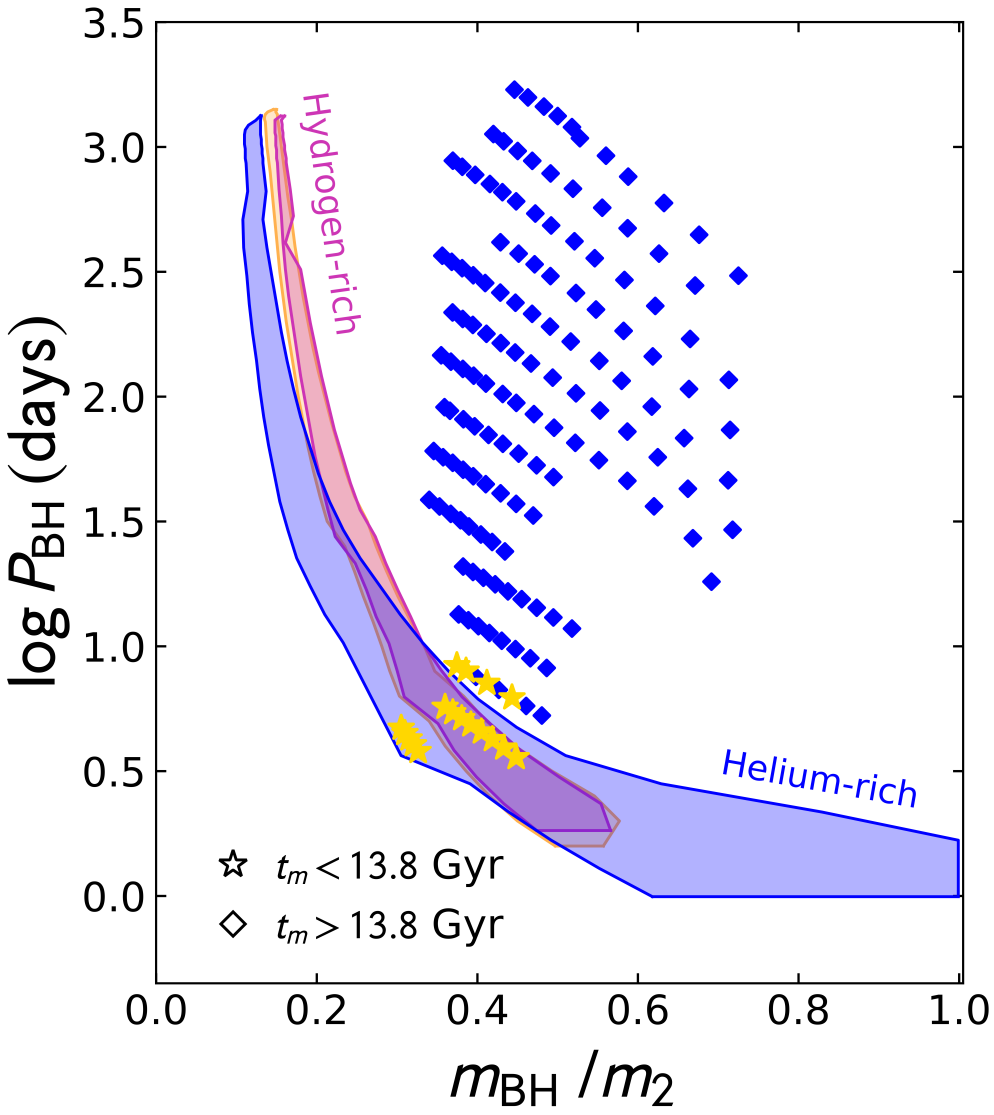

Figure 3.5: All systems experiencing stable MT at the evolutionary stage when the first black hole is formed. Stars indicate $t_{\rm merger} < 13.8$ Gyr and diamonds indicate $t_{\rm merger} > 13.8$ Gyr. Regions representing outcomes from the accretion models introduced in Chapter 2.

the markers indicating the predicted BH mergers through stable MT from the end-to-end grid (yellow stars) align with the position of the regions from the accretion models. However, we see that large areas of the regions are not populated by the results from the end-to-end evolution. This stems from the fact that this region of the parameter space does not get populated when considering a full binary evolution. Accounting for the first MT phase (stage 2) leads to a limited set of possible $P_{\rm BH}$ and $q_{\rm BH}$, excluding e.g. systems with periods above 10 days and $q_{\rm BH} > 0.5$. Compared to the non-accretion model, we see some end-to-end simulations falling outside of the region generated through this model, as well as the similar hydrogen-rich accretion model. This can be a positive indication towards the accretion model containing a higher helium mass fraction. However, we do need to keep in mind that the secondary masses of both methodologies do not match. We will now investigate the a priori choices of the accretion models that were made. The accreted mass fraction is defined as the ratio of the

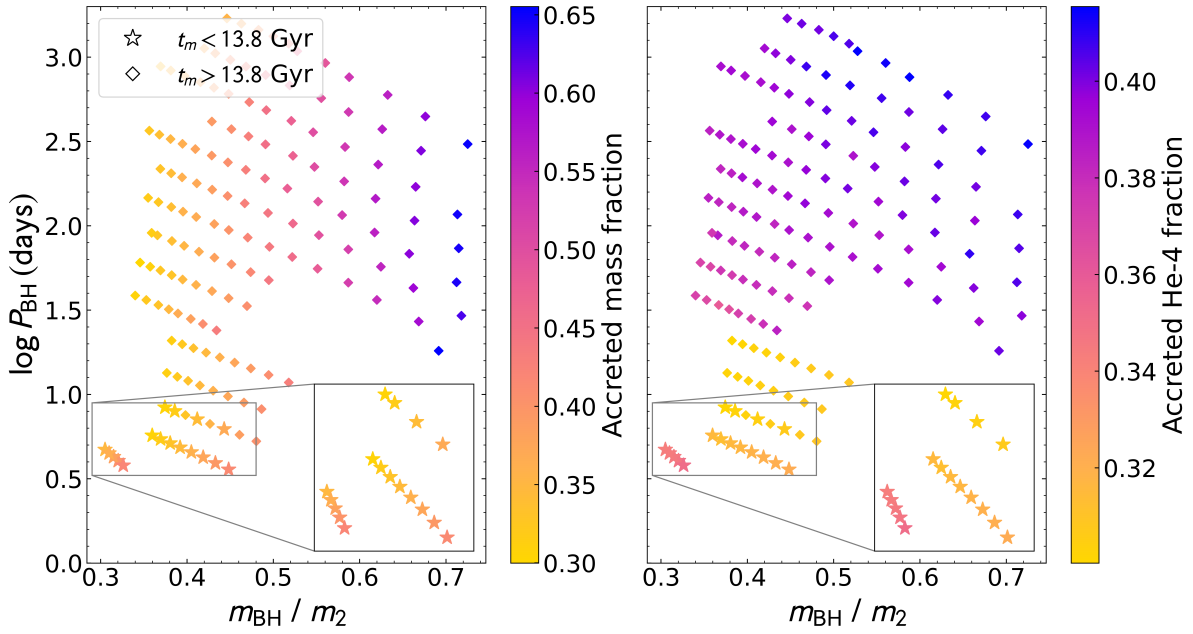

Figure 3.6: Identical parameter space as displayed in Fig. 3.3 but with an additional third dimension. Stars indicate systems experiencing stable MT with $t_{\rm merger} < 13.8$ Gyr and with diamonds if $t_{\rm merger} > 13.8$ Gyr. *Left:* Colourbar indicates the accreted mass fraction. *Right:* Colourbar indicates the accreted helium mass fraction.

accreted mass and the total mass of the secondary star, while the helium mass fraction refers to the average mass fraction of helium in the accreted material. The results for all systems that undergo stable mass transfer are depicted in the two-panel plot of Fig. 3.6.

Regarding the accreted mass fraction shown in panel one, we see that the fraction increases with mass ratio $m_{\rm BH}/m_2$. For the wide binary systems experiencing stable MT, the systems can end up with a secondary star that has an accreted mass fraction up to 0.65. However, for the predicted BH mergers (star markers), the secondary star can have an accreted mass fraction between 0.30 and 0.42. This is lower than the accreted mass fraction of 0.50 used in the accretion models. In panel two of Fig. 3.6, we show the helium mass fraction. The helium mass fraction of all depicted systems vary from 0.30 to 0.41, but for the predicted BH mergers (star markers), the accreted helium mass fraction is more limited, namely between 0.30 and 0.35. This is higher than the accreted helium mass fraction of the hydrogen-rich accretion model but lower than that of the helium-rich accretion model. Both indicate a clear jump in composition near $\log_{10} P_{\rm BH} \sim 1.5$. The helium mass fraction shows a significant increase in composition above this value. This location corresponds directly to the region in Fig. 3.2 near the single star track showing hydrogen depletion, indicating the end of the main sequence. Systems interacting after helium ignition of the primary star thus do gain a higher fraction of helium and a lower fraction of hydrogen.

We found that in Chapter 2, we decided on a reasonable accreted mass fraction, but overestimated the accreted helium mass fraction for the helium-rich model. We see that almost all models interact as case B mass transfer after the first BH formation, indicating that the accretion of helium-rich material results in more compact stars at the star+BH stage.

Chapter 4

Discussion

This chapter presents a comparison between the theoretical predictions from this thesis and the inferred orbital properties of observed single-degenerate binaries consisting of a compact object (CO) and a high mass stellar companion. Afterwards, we will give a summary of the conclusions drawn from the results presented in this thesis and discuss our findings.

4.1 Comparison with single-degenerate binary observations

To perform a comprehensive comparison between theoretical predictions and observations of single-degenerate binaries (star+CO systems), one would need to consider the following. On the one hand, for the comparison with the star+CO systems, we need a range of multiple donor masses to obtain an indication of the population distribution. In this thesis, we considered one donor mass in both methods we carried out. On the other hand, we have to take specific care of observational biases present in the considered star+CO data. One specific observational bias is that long-period star+CO binaries will be less likely detected due to a lack of X-ray emission and due to long period variations. To account for this, one should either perform a bias correction on the observational data or one should incorporate this bias effect into the theoretical predictions. Both will not be included here as this is beyond the scope of the thesis. Keeping in mind that the simulations from Chapters 2 and 3 do not offer a view of the properties' distribution of an observed star+CO sample, we present a comparison with our results and observations without accounting for biases. We consider a compiled dataset of known star+CO binaries found in literature, similarly to Picco et al. (2024).

The observations presented in Fig. 4.1 consist of high mass binaries with a compact object companion. The dataset of HMXB with a NS consists of galactic Be/X-ray+NS binaries, which we assembled from Table 1 of Tomsick and Muterspaugh (2010). This paper reports on the mass estimates of the stellar companion and assumes a mass of $1.4\ M_{\odot}$ for the NS unless another value was found in literature. For these Be/X-ray+NS systems, no uncertainties were provided. Regarding the binaries with a BH component, we depict the following six systems found in other studies (black diamonds): HD 96670 (Gomez & Grindlay, 2021), M33 X-7 (Orosz et al., 2007; Pietsch et al., 2006), LMC X-1 (Hutchings et al., 1983; Mark et al., 1969), Cyg X-1 (Miller-Jones et al., 2021), VFTS 243 (Shenar et al., 2022) and HD 130298 (Mahy et al., 2022). As opposed to Picco et al. (2024), we did not include system HD 215227 (or

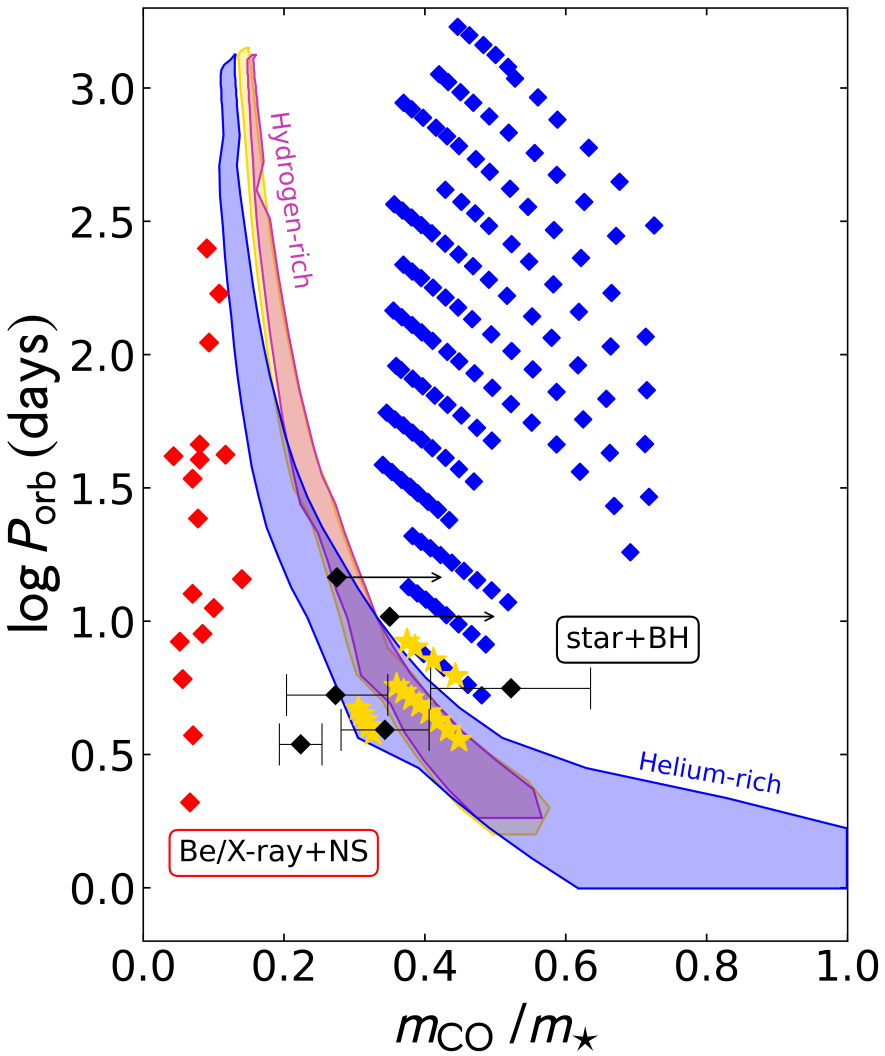

Figure 4.1: The orbital period ($\log_{10} P_{\rm orb}$) and mass ratio $m_{\rm CO}/m_\star$ between the mass of the compact object and its stellar companion of observed high and intermediate mass HMXB with a NS (red diamonds) or a BH (black markers) companion. For the latter, we account for uncertainties on the mass ratios and periods. The uncertainties on the periods are negligible within the scale of the figure. We include two inert BH binaries with massive companions for which we give an estimation on the lower limit of the mass ratio with the binary mass function. The background regions are the results of the predicted binary BH mergers from the accretion models in Chapter 2. The yellow stars and blue diamonds are the binary BH systems that undergo stable MT as predicted by the end-to-end simulations from Chapter 3.

MWC 656) (Casares et al., 2014; Janssens et al., 2023). This system was classified a Be+BH binary, but recently Rivinius et al. (2024) has reported that this is most likely a binary consisting of a Be-type star with a hot subdwarf object (sdO). System HD 130298 and VFTS 243 are reported as single line spectroscopic binaries (SB1). Therefore, we do not have constraints on a secondary radial velocity component or on the inclination of the system. We provide a minimum mass ratio calculated from the evolutionary mass of the stellar component and a minimum estimate of the mass of the BH. The minimum mass is found from the mean properties provided in Shenar et al. (2022) and Mahy et al. (2022) and the binary mass function.

The stellar and orbital parameters can be found in Table 4.1.

Fig. 4.1 depicts the orbital period $P_{\rm orb}$ and mass ratio, defined by mass of the CO ($m_{\rm CO}$) divided by the mass of the star ($m_\star$) of the observed star+CO systems together with our theoretical predictions. In this plot, we see that the star+BH binaries show up in the plane around mass ratios of $0.2 \lesssim m_{\rm CO}/m_\star \lesssim 0.6$ (accounting for error bars) and around periods of $0.50 \lesssim \log_{10} P_{\rm orb} \lesssim 1.25$. The Be/X-ray+NS systems show up at relatively low mass ratios of $m_{\rm CO}/m_\star \lesssim 0.2$, but at a broad range of periods spanning $0.25 \lesssim \log_{10} P_{\rm orb} \lesssim 2.50$.

We stress that Fig. 4.1 does not show a fully representative comparison between the theoretical results from this thesis and the star+CO observations due to the reasons cited earlier. Another caveat is that we provide theoretical predictions assuming a circular orbit, but the systems shown here all have non-zero eccentricities. In general, we do see that the star+BH binaries are close to the end-to-end BH merger predictions, as well as near the regions of the accretion models. Note that with both the accretion models from Chapter 2 and the end-to-end simulations from Chapter 3, we aim to probe binaries with a BH compact object.

Table 4.1: The stellar and orbital properties of the seven observed star+BH systems. We include the two inert star+BH binaries for which we provide a lower limit on the BH mass and thus also on the mass ratio, calculated with the binary mass function. References to each system can be found in the text.

System	$P_{\rm orb}$ (days)	$m_{\rm BH}$ $(M_\odot)$	$m_\star$ $(M_\odot)$	q
HD 215227	60.37	$3.8 - 6.9$	$10 - 16$	0.410
HD 96670	5.28388 ± 0.00046	$6.2^{+0.9}_{-0.7}$	$22.7^{+5.2}_{-3.6}$	$0.273^{+0.074}_{-0.070}$
M33 X-7	3.45301 ± 0.00002	15.65 ± 1.45	70.0 ± 6.9	0.224 ± 0.030
LMC X-1	3.90917 ± 0.00005	10.91 ± 1.41	31.79 ± 3.48	0.343 ± 0.063
Cyg X-1	5.599836 ± 0.000024	$21.2^{+2.2}_{-2.3}$	$40.6^{+7.7}_{-7.1}$	$0.522^{+0.113}_{-0.114}$
VFTS 243	10.42959 ± 0.000854	> 9.1	26 ± 2	> 0.350
HD 130298	14.62959 ± 0.000854	> 7.7	$28.0^{+5.2}_{-4.1}$	> 0.275

4.2 Conclusions & discussion

In this thesis, we carried out a study of the impact of a perturbed stellar structure due to the first mass transfer stage (stage 2 in Fig. 1.6) on the formation of double BHs through the stable MT channel. We build on the work presented in other studies (Marchant et al., 2021; Picco et al., 2024), which initialise models with a massive donor star and a CO binary. This thesis considers the fact that the donor star could have gained mass from a mass transfer episode in its earlier evolution. The structure of said donor star can be significantly altered if we were to include interaction happening before the formation of the first BH. During this interaction, the donor star in question accretes (enriched) material from the BH progenitor, which can cause different responses to the MT and therefore, different stability properties. This work provided two methodologies to investigate this effect.

In the first method, we only considered the late binary evolution stages, starting with a star+BH configuration. This donor star went through an artificial accretion process without

modelling binary evolution before the formation of the first BH. The goal of this experiment was to see how a perturbed stellar structure influences the fate of the binary BH progenitor system. This approach offers us a lot of flexibility as we can modify both the structural properties of the accretion process and the initial configuration of the star+BH binary, while comparing stability boundaries and outcomes for simulations of single degenerate binaries initialised with both stars at ZAMS. The initial configuration of the system was chosen to be comparable to the results found in literature. As the accretion models are put into practice, we see that:

- Regardless of the donor star experiencing a perturbed mass and composition due to accretion, there are still semi-degenerate binaries that span a wide range of mass ratios and orbital periods, which can produce GW signals. This confirms the robustness of the stable MT scenario as a formation channel. Specifically, as the helium mass fraction increases, the spanned area increases.

- If we calculate their relative contributions assuming a flat distribution in mass ratio and period, the amount of predicted binary BH mergers through stable MT significantly increases for the helium-rich accretion model by approximately a 3-fold. This supports the conclusion that the amount of predicted BH mergers increases for systems with a perturbed composition with a higher helium mass fraction.

- The same trend occurs when we calculate the final mass ratio of the predicted binary BH mergers, i.e., an increase of final mass ratios allowed for the helium-rich accretion model.

From this, we see that stars easily adjust to their accreted material if it is hydrogen-rich, which leads to negligible changes in their binary evolution after the formation of the first BH. When the star accretes helium-rich material, the star is not able to readjust back to a composition profile that resembles a single star composition. This leads to changes in the later evolution of the helium-rich star after the formation of the first BH, crucially influencing the stability of the second MT episode.

We performed a full end-to-end binary evolution to include the binary evolution before the formation of the first BH in the models. Doing a full one-on-one comparison with the accretion models proves difficult, but we used the results from the end-to-end simulations to question the assumptions of the accretion models. We can summarise our findings:

- For a single donor mass at a fixed metallicity, we found that $6\ \%$ of all modelled system end up as a binary BH merger out of all considered outcomes predicted by the end-to-end simulations.

- The location of the BH mergers predicted by both methods aligns in the $(\log_{10} P_{\rm BH}, q_{\rm BH})$ parameter space, but with a reduced region of $(\log_{10} P_{\rm BH}, q_{\rm BH})$ with respect to the accretion models (see Fig. 3.5). The remaining uninhabited area represents configurations that end up not being produced when modelling a full binary evolution.

- After the formation of the first BH, the BH mergers predicted by the end-to-end evolution have an accreted mass fraction between 0.30 and 0.42, which is lower than the 0.50 value of the accretion models. From this accreted mass of these systems, the helium mass fraction falls between 0.30 and 0.35. This is in the middle of the helium mass fraction considered in the hydrogen- and helium-rich accretion model.

- The interaction of the predicted BH mergers before the formation of the first BH is case A mass transfer and after, mainly case B mass transfer. This case B MT hints towards the idea that a helium-rich composition can lead towards more compact companions that overfill their Roche lobes after the main sequence.
- When comparing the calculated final mass ratios, we see that the end-to-end simulations provide a more limited range excluding unity ($0.418 < q_{\rm f} < 0.706$) compared to the ranges found for the accretion models, which only provides a lower limit.

With these results, we are able to confirm that the mass transfer stability of massive stars is dependent on the composition of the donor star, and therefore on its previous interaction phase. From the accretion models, we can conclude that the location of the stability boundary and the boundary where $t_{\rm merge} = 13.8$ Gyr are dependent on the composition of the star. Additionally, as we carry out the experiments that are the accretion models, we find that the required conditions of the binary BH mergers are qualitatively similar to those found in literature (Gallegos-Garcia et al., 2021; Marchant et al., 2021; Picco et al., 2024). However, a significant amount of helium leads to an expanded region in the considered parameter space. With the results from the end-to-end simulations, we see that it is important to include the earlier stages of the binary evolution, as doing so restricts the possible mass ratios and orbital periods at the star+BH stage significantly (see also van Son et al. 2022). We find that starting simulations at the evolutionary stage where already one BH is formed overestimates the fraction of systems that end up as merging binary BHs through stable MT as an orbital tightening mechanism.

By doing a comparison between our theoretical predictions and observations of star+BH systems, we do find binaries with a BH companion in the neighbourhood of the predicted BH mergers. Again, for a thorough comparison, one needs a population distribution from a full range of donor masses. In the considered dataset, the wide orbit systems are under-represented due to observational biases. For a detailed comparison with the theoretical framework presented in this thesis, a follow-up study needs to be done.

The amount of predicted binary BH mergers can be potentially altered by any uncertainty that was not explored and any simplifications that were made. We stress that we did not account for stellar spin or tidal coupling in the description of angular momentum. This will play a role in the resulting total angular momentum and thus also directly on the MT stability. Aside from this, we did not include the contribution of the companion to the angular momentum. In this thesis, we have highlighted an accretion process in the early evolution of a massive binary that affects the predicted binary BH mergers formed through stable MT. One can provide full predictions on the properties of both the star+BH binaries and the merging BH binaries with the methods and models presented in this thesis. As such, one can do a full comparison with electromagnetic and gravitational wave observations in the future.

Bibliography

Abbott, B. P., Abbott, R., Abbott, T. D., Abernathy, M. R., Acernese, F., Ackley, K., Adams, C., Adams, T., Addesso, P., Adhikari, R. X., Adya, V. B., Affeldt, C., Agathos, M., Agatsuma, K., Aggarwal, N., Aguiar, O. D., Aiello, L., Ain, A., Ajith, P., ... Cowart, M. J. (2016). Observation of Gravitational Waves from a Binary Black Hole Merger. *Physical Review Letters*, *116*(6), 061102. https://doi.org/10.1103/PhysRevLett.116.061102

Abbott, R., Abbott, T. D., Acernese, F., Ackley, K., Adams, C., Adhikari, N., Adhikari, R. X., Adya, V. B., Affeldt, C., Agarwal, D., Agathos, M., Agatsuma, K., Aggarwal, N., Aguiar, O. D., Aiello, L., Ain, A., Ajith, P., Akcay, S., Akutsu, T., ... Carbognani, F. (2023). GWTC-3: Compact Binary Coalescences Observed by LIGO and Virgo during the Second Part of the Third Observing Run [_eprint: 2111.03606]. *Physical Review X*, *13*(4), 041039. https://doi.org/10.1103/PhysRevX.13.041039

Abt, H. A., & Levy, S. G. (1976). Multiplicity among solar-type stars. *ApJS*, *30*, 273–306. https://doi.org/10.1086/190363

Amaro-Seoane, P., Audley, H., Babak, S., Baker, J., Barausse, E., Bender, P., Berti, E., Binetruy, P., Born, M., Bortoluzzi, D., Camp, J., Caprini, C., Cardoso, V., Colpi, M., Conklin, J., Cornish, N., Cutler, C., Danzmann, K., Dolesi, R., ... Zweifel, P. (2017). Laser Interferometer Space Antenna [_eprint: 1702.00786]. *arXiv e-prints*, arXiv:1702.00786. https://doi.org/10.48550/arXiv.1702.00786

Angulo, C., Arnould, M., Rayet, M., Descouvemont, P., Baye, D., Leclercq-Willain, C., Coc, A., Barhoumi, S., Aguer, P., Rolfs, C., Kunz, R., Hammer, J. W., Mayer, A., Paradellis, T., Kossionides, S., Chronidou, C., Spyrou, K., degl'Innocenti, S., Fiorentini, G., ... Lamehi Rachti, M. (1999). A compilation of charged-particle induced thermonuclear reaction rates. *Nuclear Physics A*, *656*(1), 3–183. https://doi.org/10.1016/S0375-9474(99)00030-5

Asplund, M., Grevesse, N., Sauval, A. J., & Scott, P. (2009). The Chemical Composition of the Sun [_eprint: 0909.0948]. *ARA&A*, *47*(1), 481–522. https://doi.org/10.1146/annurev.astro.46.060407.145222

Bardeen, J. M., Press, W. H., & Teukolsky, S. A. (1972). Rotating Black Holes: Locally Nonrotating Frames, Energy Extraction, and Scalar Synchrotron Radiation. *ApJ*, *178*, 347–370. https://doi.org/10.1086/151796

Bartos, I., Kocsis, B., Haiman, Z., & Márka, S. (2017). Rapid and Bright Stellar-mass Binary Black Hole Mergers in Active Galactic Nuclei [_eprint: 1602.03831]. *ApJ*, *835*(2), 165. https://doi.org/10.3847/1538-4357/835/2/165

Bavera, S. S., Fragos, T., Zevin, M., Berry, C. P. L., Marchant, P., Andrews, J. J., Coughlin, S., Dotter, A., Kovlakas, K., Misra, D., Serra-Perez, J. G., Qin, Y., Rocha, K. A., Román-Garza, J., Tran, N. H., & Zapartas, E. (2021). The impact of mass-transfer

physics on the observable properties of field binary black hole populations [_eprint: 2010.16333]. *A&A*, *647*, A153. https://doi.org/10.1051/0004-6361/202039804

Belczynski, K., Bulik, T., & Rudak, B. (2004). The First Stellar Binary Black Holes: The Strongest Gravitational Wave Burst Sources [_eprint: astro-ph/0403361]. *Astrophysical Journal, Letters*, *608*(1), L45–L48. https://doi.org/10.1086/422172

Belczynski, K., Dominik, M., Bulik, T., O'Shaughnessy, R., Fryer, C., & Holz, D. E. (2010). The Effect of Metallicity on the Detection Prospects for Gravitational Waves [_eprint: 1004.0386]. *ApJL*, *715*(2), L138–L141. https://doi.org/10.1088/2041-8205/715/2/L138

Belczynski, K., Holz, D. E., Bulik, T., & O'Shaughnessy, R. (2016). The first gravitational-wave source from the isolated evolution of two 40-100 Msun stars [arXiv:1602.04531 [astro-ph]]. *Nature*, *534*(7608), 512–515. https://doi.org/10.1038/nature18322

Bird, S., Cholis, I., Muñoz, J. B., Ali-Haïmoud, Y., Kamionkowski, M., Kovetz, E. D., Raccanelli, A., & Riess, A. G. (2016). Did LIGO Detect Dark Matter? [_eprint: 1603.00464]. *Physical Review Letters*, *116*(20), 201301. https://doi.org/10.1103/PhysRevLett.116.201301

Böhm-Vitense, E. (1958). Über die Wasserstoffkonvektionszone in Sternen verschiedener Effektivtemperaturen und Leuchtkräfte. Mit 5 Textabbildungen. *ZAp*, *46*, 108.

Bressan, A., & Shepherd, K. G. (2024). Evolution and final fates of low- and intermediate-mass stars [_eprint: 2412.13039]. *arXiv e-prints*, arXiv:2412.13039. https://doi.org/10.48550/arXiv.2412.13039

Broekgaarden, F. S., Banagiri, S., & Payne, E. (2024). Visualizing the Number of Existing and Future Gravitational-wave Detections from Merging Double Compact Objects [_eprint: 2303.17628]. *ApJ*, *969*(2), 108. https://doi.org/10.3847/1538-4357/ad4709

Brott, I., de Mink, S. E., Cantiello, M., Langer, N., de Koter, A., Evans, C. J., Hunter, I., Trundle, C., & Vink, J. S. (2011). Rotating massive main-sequence stars. I. Grids of evolutionary models and isochrones [_eprint: 1102.0530]. *A&A*, *530*, A115. https://doi.org/10.1051/0004-6361/201016113

Casares, J., Negueruela, I., Ribó, M., Ribas, I., Paredes, J. M., Herrero, A., & Simón-Díaz, S. (2014). A Be-type star with a black-hole companion [_eprint: 1401.3711]. *Nature*, *505*(7483), 378–381. https://doi.org/10.1038/nature12916

Chen, X., Liu, Z., & Han, Z. (2024). Binary Stars in the New Millennium [arXiv:2311.11454 [astro-ph]]. *Progress in Particle and Nuclear Physics*, *134*, 104083. https://doi.org/10.1016/j.ppnp.2023.104083

Chiosi, C., & Maeder, A. (1986). The evolution of massive stars with mass loss. *ARA&A*, *24*, 329–375. https://doi.org/10.1146/annurev.aa.24.090186.001553

Cox, J. P., & Giuli, R. T. (1968). *Principles of stellar structure*.

Crawford, J. A. (1955). On the Subgiant Components of Eclipsing Binary Systems. *ApJ*, *121*, 71. https://doi.org/10.1086/145965

Cyburt, R. H., Amthor, A. M., Ferguson, R., Meisel, Z., Smith, K., Warren, S., Heger, A., Hoffman, R. D., Rauscher, T., Sakharuk, A., Schatz, H., Thielemann, F. K., & Wiescher, M. (2010). The JINA REACLIB Database: Its Recent Updates and Impact on Type-I X-ray Bursts. *ApJS*, *189*(1), 240–252. https://doi.org/10.1088/0067-0049/189/1/240

Di Carlo, U. N., Giacobbo, N., Mapelli, M., Pasquato, M., Spera, M., Wang, L., & Haardt, F. (2019). Merging black holes in young star clusters [_eprint: 1901.00863]. *MNRAS*, *487*(2), 2947–2960. https://doi.org/10.1093/mnras/stz1453

Eggleton, P. P. (1983). Approximations to the radii of Roche lobes. *ApJ*, *268*, 368. https://doi.org/10.1086/160960

Einstein, A. (1915). The Field Equations of Gravitation. *Sitzungsber. Preuss. Akad. Wiss. Berlin (Math. Phys.)*, *1915*, 844–847.

Ferguson, J. W., Alexander, D. R., Allard, F., Barman, T., Bodnarik, J. G., Hauschildt, P. H., Heffner-Wong, A., & Tamanai, A. (2005). Low-Temperature Opacities [_eprint: astro-ph/0502045]. *ApJ*, *623*(1), 585–596. https://doi.org/10.1086/428642

Fryer, C. L. (1999). Mass Limits For Black Hole Formation [_eprint: astro-ph/9902315]. *ApJ*, *522*(1), 413–418. https://doi.org/10.1086/307647

Fuller, G. M., Fowler, W. A., & Newman, M. J. (1985). Stellar weak interaction rates for intermediate-mass nuclei. IV - Interpolation procedures for rapidly varying lepton capture rates using effective log (ft)-values. *ApJ*, *293*, 1–16. https://doi.org/10.1086/163208

Gallegos-Garcia, M., Berry, C. P. L., Marchant, P., & Kalogera, V. (2021). Binary Black Hole Formation with Detailed Modeling: Stable Mass Transfer Leads to Lower Merger Rates [_eprint: 2107.05702]. *ApJ*, *922*(2), 110. https://doi.org/10.3847/1538-4357/ac2610

Geen, S., Agrawal, P., Crowther, P. A., Keller, B. W., de Koter, A., Keszthelyi, Z., van de Voort, F., Ali, A. A., Backs, F., Bonne, L., Brugaletta, V., Derkink, A., Ekström, S., Fichtner, Y. A., Grassitelli, L., Götberg, Y., Higgins, E. R., Laplace, E., You Liow, K., … Winch, E. (2023). Bringing Stellar Evolution and Feedback Together: Summary of Proposals from the Lorentz Center Workshop [_eprint: 2301.13611]. *PASP*, *135*(1044), 021001. https://doi.org/10.1088/1538-3873/acb6b5

Gomez, S., & Grindlay, J. E. (2021). Optical Analysis and Modeling of HD96670, a New Black Hole X-Ray Binary Candidate [_eprint: 2211.04518]. *ApJ*, *913*(1), 48. https://doi.org/10.3847/1538-4357/abf24c

Hall, E. D. (2022). Cosmic Explorer: A Next-Generation Ground-Based Gravitational-Wave Observatory. *Galaxies*, *10*(4), 90. https://doi.org/10.3390/galaxies10040090

Hamann, W. .-., Koesterke, L., & Wessolowski, U. (1995). Spectral analyses of the Galactic Wolf-Rayet stars: Hydrogen-helium abundances and improved stellar parameters for the WN class. *A&A*, *299*, 151.

Heger, A., Fryer, C. L., Woosley, S. E., Langer, N., & Hartmann, D. H. (2003). How Massive Single Stars End Their Life [_eprint: astro-ph/0212469]. *ApJ*, *591*(1), 288–300. https://doi.org/10.1086/375341

Herwig, F. (2000). The evolution of AGB stars with convective overshoot [_eprint: astro-ph/0007139]. *A&A*, *360*, 952–968. https://doi.org/10.48550/arXiv.astro-ph/0007139

Hjellming, M. S., & Webbink, R. F. (1987). Thresholds for Rapid Mass Transfer in Binary System. I. Polytropic Models. *ApJ*, *318*, 794. https://doi.org/10.1086/165412

Hulse, R. A., & Taylor, J. H. (1975). Discovery of a pulsar in a binary system. *ApJL*, *195*, L51–L53. https://doi.org/10.1086/181708

Hutchings, J. B., Crampton, D., & Cowley, A. P. (1983). LMC X-1: Another Massive Binary? *IAU Circ.*, *3791*, 3.

Iglesias, C. A., & Rogers, F. J. (1993). Radiative opacities for carbon- and oxygen-rich mixtures. *ApJ*, *412*, 752–760. https://doi.org/10.1086/172958

Iglesias, C. A., & Rogers, F. J. (1996). Updated Opal Opacities. *ApJ*, *464*, 943. https://doi.org/10.1086/177381

Inayoshi, K., Hirai, R., Kinugawa, T., & Hotokezaka, K. (2017). Formation pathway of Population III coalescing binary black holes through stable mass transfer [_eprint: 1701.04823]. *MNRAS*, *468*(4), 5020–5032. https://doi.org/10.1093/mnras/stx757

Irwin, A. W. (2004). The FreeEOS Code for Calculating the Equation of State for Stellar Interiors. http://freeeos.sourceforge.net/

Janssens, S., Shenar, T., Degenaar, N., Bodensteiner, J., Sana, H., Audenaert, J., & Frost, A. J. (2023). MWC 656 is unlikely to contain a black hole [_eprint: 2308.08642]. *A&A*, *677*, L9. https://doi.org/10.1051/0004-6361/202347318

Jermyn, A. S., Bauer, E. B., Schwab, J., Farmer, R., Ball, W. H., Bellinger, E. P., Dotter, A., Joyce, M., Marchant, P., Mombarg, J. S. G., Wolf, W. M., Sunny Wong, T. L., Cinquegrana, G. C., Farrell, E., Smolec, R., Thoul, A., Cantiello, M., Herwig, F., Toloza, O., . . . Timmes, F. X. (2023). Modules for Experiments in Stellar Astrophysics (MESA): Time-dependent Convection, Energy Conservation, Automatic Differentiation, and Infrastructure [_eprint: 2208.03651]. *ApJS*, *265*(1), 15. https://doi.org/10.3847/1538-4365/acae8d

Jermyn, A. S., Schwab, J., Bauer, E., Timmes, F. X., & Potekhin, A. Y. (2021). Skye: A Differentiable Equation of State [_eprint: 2104.00691]. *ApJ*, *913*(1), 72. https://doi.org/10.3847/1538-4357/abf48e

King, A. R., Schenker, K., Kolb, U., & Davies, M. B. (2001). The minimum orbital period in thermal time-scale mass transfer [_eprint: astro-ph/0009062]. *MNRAS*, *321*(2), 327–332. https://doi.org/10.1046/j.1365-8711.2001.04002.x

Kinugawa, T., Inayoshi, K., Hotokezaka, K., Nakauchi, D., & Nakamura, T. (2014). Possible indirect confirmation of the existence of Pop III massive stars by gravitational wave [_eprint: 1402.6672]. *MNRAS*, *442*(4), 2963–2992. https://doi.org/10.1093/mnras/stu1022

Kippenhahn, R., Ruschenplatt, G., & Thomas, H. .-. (1980). The time scale of thermohaline mixing in stars. *A&A*, *91*(1-2), 175–180.

Kippenhahn, R., & Weigert, A. (1967). Entwicklung in engen Doppelsternsystemen I. Massenaustausch vor und nach Beendigung des zentralen Wasserstoff-Brennens. *ZAp*, *65*, 251.

Klencki, J., Nelemans, G., Istrate, A. G., & Chruslinska, M. (2021). It has to be cool: Supergiant progenitors of binary black hole mergers from common-envelope evolution [_eprint: 2006.11286]. *A&A*, *645*, A54. https://doi.org/10.1051/0004-6361/202038707

Kulkarni, S. R., Hut, P., & McMillan, S. (1993). Stellar black holes in globular clusters. *Nature*, *364*(6436), 421–423. https://doi.org/10.1038/364421a0

Langanke, K., & Martínez-Pinedo, G. (2000). Shell-model calculations of stellar weak interaction rates: II. Weak rates for nuclei in the mass range /A=45-65 in supernovae environments [_eprint: nucl-th/0001018]. *Nuclear Physics A*, *673*, 481–508. https://doi.org/10.1016/S0375-9474(00)00131-7

Langer, N., Fricke, K. J., & Sugimoto, D. (1983). Semiconvective diffusion and energy transport. *A&A*, *126*(1), 207.

Lauterborn, D. (1970). Evolution with mass exchange of case C for a binary system of total mass 7 M sun. *A&A*, *7*, 150.

Lechien, T., de Mink, S. E., Valli, R., Rubio, A. C., van Son, L. A. C., Klement, R., Jin, H., & Pols, O. (2025). Binary stars take what they get: Evidence for Efficient Mass Transfer from Stripped Stars with Rapidly Rotating Companions [_eprint: 2505.14780]. *arXiv e-prints*, arXiv:2505.14780. https://doi.org/10.48550/arXiv.2505.14780

Ledoux, P. (1947). Stellar Models with Convection and with Discontinuity of the Mean Molecular Weight. *ApJ*, *105*, 305. https://doi.org/10.1086/144905

Maeder, A. (1987). Evidences for a bifurcation in massive star evolution. The ON-blue stragglers. *A&A*, *178*, 159–169.

Maggiore, M., Van Den Broeck, C., Bartolo, N., Belgacem, E., Bertacca, D., Bizouard, M. A., Branchesi, M., Clesse, S., Foffa, S., García-Bellido, J., Grimm, S., Harms, J., Hinderer, T., Matarrese, S., Palomba, C., Peloso, M., Ricciardone, A., & Sakellariadou, M. (2020). Science case for the Einstein telescope [_eprint: 1912.02622]. *Journal of Cosmology and Astroparticle Physics*, *2020*(3), 050. https://doi.org/10.1088/1475-7516/2020/03/050

Mahy, L., Sana, H., Shenar, T., Sen, K., Langer, N., Marchant, P., Abdul-Masih, M., Banyard, G., Bodensteiner, J., Bowman, D. M., Dsilva, K., Fabry, M., Hawcroft, C., Janssens, S., Van Reeth, T., & Eldridge, C. (2022). Identifying quiescent compact objects in massive Galactic single-lined spectroscopic binaries [_eprint: 2207.07752]. *A&A*, *664*, A159. https://doi.org/10.1051/0004-6361/202243147

Manchester, R. N., & IPTA. (2013). The International Pulsar Timing Array [_eprint: 1309.7392]. *Classical and Quantum Gravity*, *30*(22), 224010. https://doi.org/10.1088/0264-9381/30/22/224010

Mandel, I., & de Mink, S. E. (2016). Merging binary black holes formed through chemically homogeneous evolution in short-period stellar binaries [_eprint: 1601.00007]. *MNRAS*, *458*(3), 2634–2647. https://doi.org/10.1093/mnras/stw379

Mandel, I., & Farmer, A. (2022). Merging stellar-mass binary black holes [arXiv:1806.05820 [astro-ph, physics:gr-qc]]. *Physics Reports*, *955*, 1–24. https://doi.org/10.1016/j.physrep.2022.01.003

Mapelli, M. (2021). Formation Channels of Single and Binary Stellar-Mass Black Holes. In C. Bambi, S. Katsanevas, & K. D. Kokkotas (Eds.), *Handbook of Gravitational Wave Astronomy* (p. 16). https://doi.org/10.1007/978-981-15-4702-7_16-1

Marchant, P. (2025). Evolution of binary stars [_eprint: 2503.16099]. *arXiv e-prints*, arXiv:2503.16099. https://doi.org/10.48550/arXiv.2503.16099

Marchant, P., & Bodensteiner, J. (2024). The Evolution of Massive Binary Stars. *Annual Review of Astronomy and Astrophysics*. https://doi.org/10.1146/annurev-astro-052722-105936

Marchant, P., Langer, N., Podsiadlowski, P., Tauris, T. M., de Mink, S., Mandel, I., & Moriya, T. J. (2017). Ultra-luminous X-ray sources and neutron-star-black-hole mergers from very massive close binaries at low metallicity [_eprint: 1705.04734]. *A&A*, *604*, A55. https://doi.org/10.1051/0004-6361/201630188

Marchant, P., Langer, N., Podsiadlowski, P., Tauris, T. M., & Moriya, T. J. (2016). A new route towards merging massive black holes [_eprint: 1601.03718]. *A&A*, *588*, A50. https://doi.org/10.1051/0004-6361/201628133

Marchant, P., Pappas, K. M. W., Gallegos-Garcia, M., Berry, C. P. L., Taam, R. E., Kalogera, V., & Podsiadlowski, P. (2021). The role of mass transfer and common envelope evolution in the formation of merging binary black holes [arXiv:2103.09243 [astro-ph]]. *Astronomy & Astrophysics*, *650*, A107. https://doi.org/10.1051/0004-6361/202039992

Mark, H., Price, R., Rodrigues, R., Seward, F. D., & Swift, C. D. (1969). Detection of X-Rays from the Large Magellanic Cloud. *ApJL*, *155*, L143. https://doi.org/10.1086/180322

McKernan, B., Ford, K. E. S., Kocsis, B., Lyra, W., & Winter, L. M. (2014). Intermediate-mass black holes in AGN discs - II. Model predictions and observational constraints [_eprint: 1403.6433]. *MNRAS*, *441*(1), 900–909. https://doi.org/10.1093/mnras/stu553

Mestel, L. (1968). Magnetic braking by a stellar wind-I. *MNRAS*, *138*, 359. https://doi.org/10.1093/mnras/138.3.359

Miller-Jones, J. C. A., Bahramian, A., Orosz, J. A., Mandel, I., Gou, L., Maccarone, T. J., Neijssel, C. J., Zhao, X., Ziółkowski, J., Reid, M. J., Uttley, P., Zheng, X., Byun, D.-Y., Dodson, R., Grinberg, V., Jung, T., Kim, J.-S., Marcote, B., Markoff, S., ...

Wilms, J. (2021). Cygnus X-1 contains a 21-solar mass black hole—Implications for massive star winds [_eprint: 2102.09091]. *Science*, *371*(6533), 1046–1049. https://doi.org/10.1126/science.abb3363

Misra, D., Fragos, T., Tauris, T. M., Zapartas, E., & Aguilera-Dena, D. R. (2020). The origin of pulsating ultra-luminous X-ray sources: Low- and intermediate-mass X-ray binaries containing neutron star accretors [_eprint: 2004.01205]. *A&A*, *642*, A174. https://doi.org/10.1051/0004-6361/202038070

Moore, C. J., Cole, R. H., & Berry, C. P. L. (2015). Gravitational-wave sensitivity curves [arXiv:1408.0740 [gr-qc]]. *Classical and Quantum Gravity*, *32*(1), 015014. https://doi.org/10.1088/0264-9381/32/1/015014

Neijssel, C. J., Vigna-Gómez, A., Stevenson, S., Barrett, J. W., Gaebel, S. M., Broekgaarden, F. S., de Mink, S. E., Szécsi, D., Vinciguerra, S., & Mandel, I. (2019). The effect of the metallicity-specific star formation history on double compact object mergers [_eprint: 1906.08136]. *MNRAS*, *490*(3), 3740–3759. https://doi.org/10.1093/mnras/stz2840

Nieuwenhuijzen, H., & de Jager, C. (1990). Parametrization of stellar rates of mass loss as functions of the fundamental stellar parameters M, L, and R. *A&A*, *231*, 134–136.

Nomoto, K., Kobayashi, C., & Tominaga, N. (2013). Nucleosynthesis in Stars and the Chemical Enrichment of Galaxies. *ARA&A*, *51*(1), 457–509. https://doi.org/10.1146/annurev-astro-082812-140956

Oda, T., Hino, M., Muto, K., Takahara, M., & Sato, K. (1994). Rate Tables for the Weak Processes of sd-Shell Nuclei in Stellar Matter. *Atomic Data and Nuclear Data Tables*, *56*, 231–403. https://doi.org/10.1006/adnd.1994.1007

Orosz, J. A., McClintock, J. E., Bailyn, C. D., Remillard, R. A., Pietsch, W., & Narayan, R. (2007). Dynamical Evidence for a Black Hole in the Eclipsing X-ray Binary M33 X-7. *The Astronomer's Telegram*, *977*, 1.

Paczynski, B. (1976, January). Common Envelope Binaries. In P. Eggleton, S. Mitton, & J. Whelan (Eds.), *Structure and Evolution of Close Binary Systems* (p. 75, Vol. 73).

Paxton, B., Bildsten, L., Dotter, A., Herwig, F., Lesaffre, P., & Timmes, F. (2011). Modules for Experiments in Stellar Astrophysics (MESA) [_eprint: 1009.1622]. *ApJS*, *192*, 3. https://doi.org/10.1088/0067-0049/192/1/3

Paxton, B., Cantiello, M., Arras, P., Bildsten, L., Brown, E. F., Dotter, A., Mankovich, C., Montgomery, M. H., Stello, D., Timmes, F. X., & Townsend, R. (2013). Modules for Experiments in Stellar Astrophysics (MESA): Planets, Oscillations, Rotation, and Massive Stars [_eprint: 1301.0319]. *ApJS*, *208*, 4. https://doi.org/10.1088/0067-0049/208/1/4

Paxton, B., Marchant, P., Schwab, J., Bauer, E. B., Bildsten, L., Cantiello, M., Dessart, L., Farmer, R., Hu, H., Langer, N., Townsend, R. H. D., Townsley, D. M., & Timmes, F. X. (2015). Modules for Experiments in Stellar Astrophysics (MESA): Binaries, Pulsations, and Explosions [_eprint: 1506.03146]. *ApJS*, *220*, 15. https://doi.org/10.1088/0067-0049/220/1/15

Paxton, B., Schwab, J., Bauer, E. B., Bildsten, L., Blinnikov, S., Duffell, P., Farmer, R., Goldberg, J. A., Marchant, P., Sorokina, E., Thoul, A., Townsend, R. H. D., & Timmes, F. X. (2018). Modules for Experiments in Stellar Astrophysics (MESA): Convective Boundaries, Element Diffusion, and Massive Star Explosions [_eprint: 1710.08424]. *ApJS*, *234*, 34. https://doi.org/10.3847/1538-4365/aaa5a8

Paxton, B., Smolec, R., Schwab, J., Gautschy, A., Bildsten, L., Cantiello, M., Dotter, A., Farmer, R., Goldberg, J. A., Jermyn, A. S., Kanbur, S. M., Marchant, P., Thoul, A.,

Townsend, R. H. D., Wolf, W. M., Zhang, M., & Timmes, F. X. (2019). Modules for Experiments in Stellar Astrophysics (MESA): Pulsating Variable Stars, Rotation, Convective Boundaries, and Energy Conservation [_eprint: 1903.01426]. *ApJS*, *243*(1), 10. https://doi.org/10.3847/1538-4365/ab2241

Peters, P. C. (1964). Gravitational Radiation and the Motion of Two Point Masses. *Physical Review*, *136*(4B), 1224–1232. https://doi.org/10.1103/PhysRev.136.B1224

Picco, A., Marchant, P., Sana, H., & Nelemans, G. (2024). Forming merging double compact objects with stable mass transfer. *Astronomy & Astrophysics*, *681*, A31. https://doi.org/10.1051/0004-6361/202347090

Pietsch, W., Haberl, F., Sasaki, M., Gaetz, T. J., Plucinsky, P. P., Ghavamian, P., Long, K. S., & Pannuti, T. G. (2006). M33 X-7: ChASeM33 Reveals the First Eclipsing Black Hole X-Ray Binary [_eprint: astro-ph/0603698]. *ApJ*, *646*(1), 420–428. https://doi.org/10.1086/504704

Portegies Zwart, S. F., & McMillan, S. L. W. (2000). Black Hole Mergers in the Universe [_eprint: astro-ph/9910061]. *Astrophysical Journal, Letters*, *528*(1), L17–L20. https://doi.org/10.1086/312422

Potekhin, A. Y., & Chabrier, G. (2010). Thermodynamic Functions of Dense Plasmas: Analytic Approximations for Astrophysical Applications [_eprint: 1001.0690]. *Contributions to Plasma Physics*, *50*, 82–87. https://doi.org/10.1002/ctpp.201010017

Ritter, H. (1988). Turning on and off mass transfer in cataclysmic binaries. *A&A*, *202*, 93–100.

Rivinius, T., Klement, R., Chojnowski, S. D., Baade, D., Shepard, K., & Hadrava, P. (2024, January). MWC 656: A Be+BH or a Be+sdO? [_eprint: 2208.12315]. In J. Mackey, J. S. Vink, & N. St-Louis (Eds.), *Massive Stars Near and Far* (pp. 332–333, Vol. 361). https://doi.org/10.1017/S1743921322002976

Rocha, K. A., Hur, R., Kalogera, V., Gossage, S., Sun, M., Doctor, Z., Andrews, J. J., Bavera, S. S., Briel, M. M., Fragos, T., Kovlakas, K., Kruckow, M. U., Misra, D., Xing, Z., & Zapartas, E. (2025). Mass Transfer in Eccentric Orbits with Self-consistent Stellar Evolution [_eprint: 2411.11840]. *ApJ*, *983*(1), 39. https://doi.org/10.3847/1538-4357/adb970

Rodriguez, C. L., Morscher, M., Pattabiraman, B., Chatterjee, S., Haster, C.-J., & Rasio, F. A. (2015). Binary Black Hole Mergers from Globular Clusters: Implications for Advanced LIGO [_eprint: 1505.00792]. *Physical Review Letters*, *115*(5), 051101. https://doi.org/10.1103/PhysRevLett.115.051101

Rogers, F. J., & Nayfonov, A. (2002). Updated and Expanded OPAL Equation-of-State Tables: Implications for Helioseismology. *ApJ*, *576*, 1064–1074. https://doi.org/10.1086/341894

Sana, H., de Mink, S. E., de Koter, A., Langer, N., Evans, C. J., Gieles, M., Gosset, E., Izzard, R. G., Le Bouquin, J. .-., & Schneider, F. R. N. (2012). Binary Interaction Dominates the Evolution of Massive Stars [_eprint: 1207.6397]. *Science*, *337*(6093), 444. https://doi.org/10.1126/science.1223344

Sana, H., & Vrancken, J. (2025). Observing Binaries [_eprint: 2504.00548]. *arXiv e-prints*, arXiv:2504.00548. https://doi.org/10.48550/arXiv.2504.00548

Sasaki, M., Suyama, T., Tanaka, T., & Yokoyama, S. (2018). Primordial black holes—perspectives in gravitational wave astronomy [_eprint: 1801.05235]. *Classical and Quantum Gravity*, *35*(6), 063001. https://doi.org/10.1088/1361-6382/aaa7b4

Saumon, D., Chabrier, G., & van Horn, H. M. (1995). An Equation of State for Low-Mass Stars and Giant Planets. *ApJS*, *99*, 713. https://doi.org/10.1086/192204

Schatzman, E. (1962). A theory of the role of magnetic activity during star formation. *Annales d'Astrophysique*, *25*, 18.

Schneider, F. R. N., Podsiadlowski, P., & Laplace, E. (2023). Bimodal Black Hole Mass Distribution and Chirp Masses of Binary Black Hole Mergers [_eprint: 2305.02380]. *ApJL*, *950*(2), L9. https://doi.org/10.3847/2041-8213/acd77a

Sepinsky, J. F., Willems, B., Kalogera, V., & Rasio, F. A. (2010). Interacting Binaries with Eccentric Orbits. III. Orbital Evolution due to Direct Impact and Self-Accretion [_eprint: 1005.0625]. *ApJ*, *724*(1), 546–558. https://doi.org/10.1088/0004-637X/724/1/546

Shenar, T., Sana, H., Mahy, L., Maíz Apellániz, J., Crowther, P. A., Gromadzki, M., Herrero, A., Langer, N., Marchant, P., Schneider, F. R. N., Sen, K., Soszyński, I., & Toonen, S. (2022). The Tarantula Massive Binary Monitoring. VI. Characterisation of hidden companions in 51 single-lined O-type binaries: A flat mass-ratio distribution and black-hole binary candidates [_eprint: 2207.07674]. *A&A*, *665*, A148. https://doi.org/10.1051/0004-6361/202244245

Sigurdsson, S., & Hernquist, L. (1993). Primordial black holes in globular clusters. *Nature*, *364*(6436), 423–425. https://doi.org/10.1038/364423a0

Soberman, G. E., Phinney, E. S., & van den Heuvel, E. P. J. (1997). Stability criteria for mass transfer in binary stellar evolution. [_eprint: astro-ph/9703016]. *A&A*, *327*, 620–635. https://doi.org/10.48550/arXiv.astro-ph/9703016

Stone, N. C., Metzger, B. D., & Haiman, Z. (2017). Assisted inspirals of stellar mass black holes embedded in AGN discs: Solving the 'final au problem' [_eprint: 1602.04226]. *MNRAS*, *464*(1), 946–954. https://doi.org/10.1093/mnras/stw2260

Tauris, T. M., & van den Heuvel, E. P. J. (2023). *Physics of Binary Star Evolution. From Stars to X-ray Binaries and Gravitational Wave Sources*. https://doi.org/10.48550/arXiv.2305.09388

Timmes, F. X., & Swesty, F. D. (2000). The Accuracy, Consistency, and Speed of an Electron-Positron Equation of State Based on Table Interpolation of the Helmholtz Free Energy. *ApJS*, *126*(2), 501–516. https://doi.org/10.1086/313304

Tomsick, J. A., & Muterspaugh, M. W. (2010). Masses of Neutron Stars in High-mass X-ray Binaries with Optical Astrometry [_eprint: 1006.4665]. *ApJ*, *719*(1), 958–965. https://doi.org/10.1088/0004-637X/719/1/958

van Son, L. A. C., de Mink, S. E., Renzo, M., Justham, S., Zapartas, E., Breivik, K., Callister, T., Farr, W. M., & Conroy, C. (2022). No Peaks without Valleys: The Stable Mass Transfer Channel for Gravitational-wave Sources in Light of the Neutron Star-Black Hole Mass Gap [_eprint: 2209.13609]. *ApJ*, *940*(2), 184. https://doi.org/10.3847/1538-4357/ac9b0a

van den Heuvel, E. P. J., Portegies Zwart, S. F., & de Mink, S. E. (2017). Forming short-period Wolf-Rayet X-ray binaries and double black holes through stable mass transfer [_eprint: 1701.02355]. *MNRAS*, *471*(4), 4256–4264. https://doi.org/10.1093/mnras/stx1430

Verbunt, F., & Phinney, E. S. (1995). Tidal circularization and the eccentricity of binaries containing giant stars. *A&A*, *296*, 709.

Vink, J. S. (2022). Theory and Diagnostics of Hot Star Mass Loss [_eprint: 2109.08164]. *\araa*, *60*, 203–246. https://doi.org/10.1146/annurev-astro-052920-094949

Vink, J. S., de Koter, A., & Lamers, H. J. G. L. M. (2001). Mass-loss predictions for O and B stars as a function of metallicity [_eprint: astro-ph/0101509]. *A&A*, *369*, 574–588. https://doi.org/10.1051/0004-6361:20010127

Yoon, S. .-., Woosley, S. E., & Langer, N. (2010). Type Ib/c Supernovae in Binary Systems. I. Evolution and Properties of the Progenitor Stars [_eprint: 1004.0843]. *ApJ*, *725*(1), 940–954. https://doi.org/10.1088/0004-637X/725/1/940

Zevin, M., Bavera, S. S., Berry, C. P. L., Kalogera, V., Fragos, T., Marchant, P., Rodriguez, C. L., Antonini, F., Holz, D. E., & Pankow, C. (2021). One Channel to Rule Them All? Constraining the Origins of Binary Black Holes Using Multiple Formation Pathways [_eprint: 2011.10057]. *ApJ*, *910*(2), 152. https://doi.org/10.3847/1538-4357/abe40e

Appendices

Appendix for Chapter 2: Non-accreting model

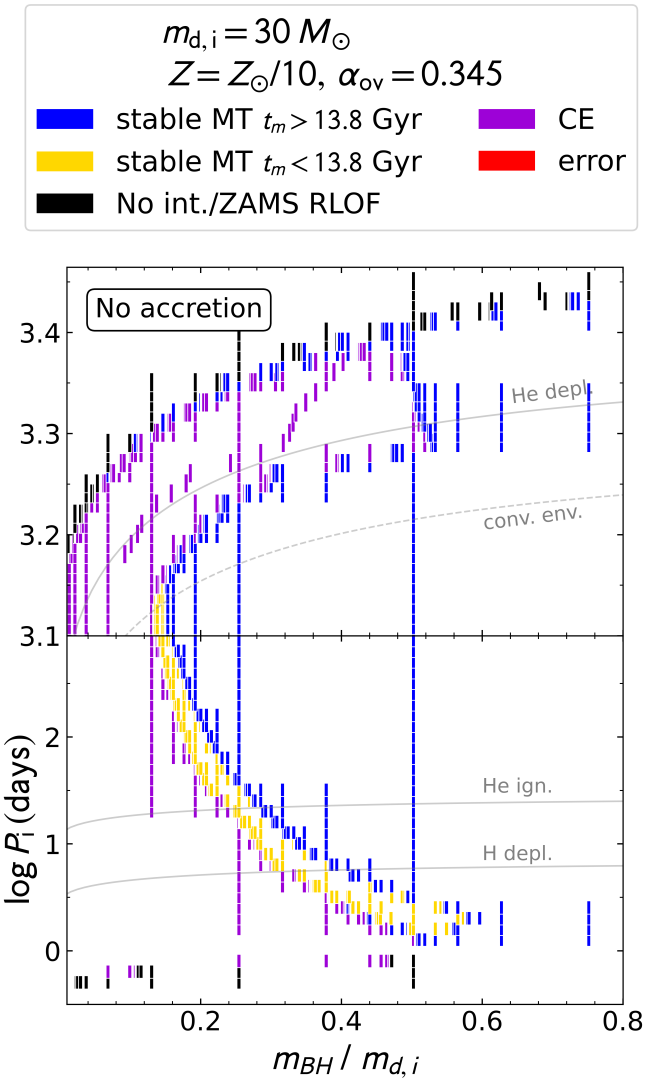

Figure A1: Summary of final outcomes of the simulations using the bisection algorithm to find the stability boundary and the boundary where $t_{\rm merge} = 13.8$ Gyr. Horizontal lines indicate different evolutionary stages of a single star with the same initial mass as the donor star. Solid lines mark hydrogen depletion and helium ignition. Dashed line in the upper panels show where the star starts to have a 0.05 fraction of the convective envelope.

Appendix for Chapter 3: Masses of the secondary component at formation first BH

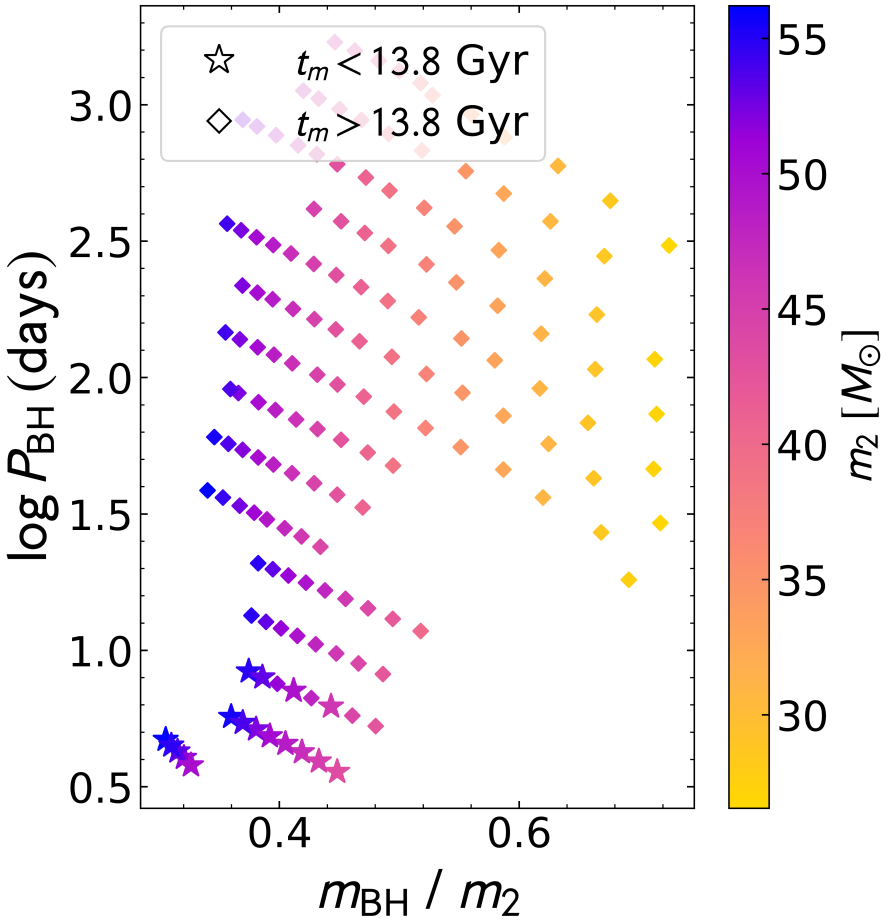

Figure A2: Identical parameter space as displayed in Fig. 3.3 but with an additional third dimension. Stars indicate systems experiencing stable MT with $t_{\rm merger} < 13.8$ Gyr and with diamonds if $t_{\rm merger} > 13.8$ Gyr. Colourbar indicates the mass of the secondary component.

DEPARTMENT OF PHYSICS AND ASTRONOMY
Celestijnenlaan 200D bus 2401
3001 LEUVEN, BELGIË
tel. + 32 16 32 71 24
www.ster.kuleuven.be